Bioorganic Chemistry 145 (2024) 107221

Contents lists available at ScienceDirect

Bioorganic Chemistry

journal homepage: www.elsevier.com/locate/bioorg

Novel spiroindoline derivatives targeting aldose reductase against diabetic complications: Bioactivity, cytotoxicity, and molecular modeling studies

Özcan Güleç [a], Cüneyt Türkeş [b,*,1], Mustafa Arslan [a,*,2], Yeliz Demir [c], Busra Dincer [d], Abdulilah Ece [e], Ömer İrfan Küfrevioğlu [f], Şükrü Beydemir [g,h]

[a] Department of Chemistry, Faculty of Arts and Sciences, Sakarya University, 54187 Sakarya, Turkey
[b] Department of Biochemistry, Faculty of Pharmacy, Erzincan Binali Yıldırım University, 24002 Erzincan, Turkey
[c] Department of Pharmacy Services, Nihat Delibalta Göle Vocational High School, Ardahan University, 75700 Ardahan, Turkey
[d] Department of Pharmacology, Faculty of Pharmacy, Ondokuz Mayıs University, 55020 Samsun, Turkey
[e] Department of Pharmaceutical Chemistry, Faculty of Pharmacy, Biruni University, 34010 İstanbul, Turkey
[f] Department of Chemistry, Faculty of Sciences, Atatürk University, 25240 Erzurum, Turkey
[g] Department of Biochemistry, Faculty of Pharmacy, Anadolu University, 26470 Eskişehir, Turkey
[h] Bilecik Şeyh Edebali University, 11230 Bilecik, Turkey

ARTICLE INFO

Keywords:
Aldose reductase
Spiroindoline
Diabetic complication
Inhibitor
Cytotoxicity
In silico study

ABSTRACT

Despite significant developments in therapeutic strategies, Diabetes Mellitus remains an increasing concern, leading to various complications, e.g., cataracts, neuropathy, retinopathy, nephropathy, and several cardiovascular diseases. The polyol pathway, which involves Aldose reductase (AR) as a critical enzyme, has been focused on by many researchers as a target for intervention. On the other hand, spiroindoline-based compounds possess remarkable biological properties. This guided us to synthesize novel spiroindoline oxadiazolyl-based acetate derivatives and investigate their biological activities. The synthesized molecules' structures were confirmed herein, using IR, NMR (^{1}H and ^{13}C), and Mass spectroscopy. All compounds were potent inhibitors with K_I constants spanning from 0.186 ± 0.020 μM to 0.662 ± 0.042 μM versus AR and appeared as better inhibitors than the clinically used drug, Epalrestat (EPR, K_I: 0.841 ± 0.051 μM). Besides its remarkable inhibitory profile compared to EPR, compound **6k** (K_I: 0.186 ± 0.020 μM) was also determined to have an unusual pharmacokinetic profile. The results showed that **6k** had less cytotoxic effect on normal mouse fibroblast (L929) cells (IC_{50} of 569.58 ± 0.80 μM) and reduced the viability of human breast adenocarcinoma (MCF-7) cells (IC_{50} of 110.87 ± 0.42 μM) more than the reference drug Doxorubicin (IC_{50}s of 98.26 ± 0.45 μM and 158.49 ± 2.73 μM, respectively), thus exhibiting more potent anticancer activity. Moreover, molecular dynamic simulations for 200 ns were conducted to predict the docked complex's stability and reveal significant amino acid residues that **6k** interacts with throughout the simulation.

1. Introduction

Aldose reductase (E.C.1.1.1.21, AR) is considered an NADPH-dependent oxidoreductase, playing a crucial role in the catalytic conversion of glucose to sorbitol during a hyperglycemic state. This enzyme is a pivotal component of the polyol pathway, which serves as an alternative route for metabolizing a small proportion of non-phosphorylated glucose. The subsequent reduction of sorbitol into fructose is facilitated by sorbitol dehydrogenase. It is important to note that osmotic stress, associated with sorbitol deposition and redox imbalance following NADPH depletion, significantly contributes to cell and organ damages. This ultimately leads to the formation of cataracts

Abbreviations: AIC, Akaike information criterion; AR, Aldose reductase; ATCC, American type culture collection; DMF, dimethylformamide; DMSO, dimethylsulfoxide; DOX, Doxorubicin; EPR, Epalrestat; K_I, enzyme inhibition constants; R^2, K_I coefficient of determination; OPLS, optimal potential liquid simulations; SARs, structure–activity relationships; TBAB, tetrabutylammonium bromide.

* Corresponding authors.
E-mail addresses: cuneyt.turkes@erzincan.edu.tr (C. Türkeş), marslan@sakarya.edu.tr (M. Arslan).
[1] ORCID ID: 0000-0002-2932-2789.
[2] ORCID ID: 0000-0003-0796-4374.

https://doi.org/10.1016/j.bioorg.2024.107221
Received 30 October 2023; Received in revised form 1 February 2024; Accepted 16 February 2024
Available online 19 February 2024

[1], neuropathy [2], retinopathy [3], nephropathy [4], and other diabetic complications [5], and several cardiovascular diseases, such as congestive heart failure, myocardial ischemia, cardiac hypertrophy, and cardiomyopathy [6] (Fig. 1). Additionally, multiple malignancies, including breast, liver, cervical, ovarian, and rectal cancers, are postulated to stem from augmented generation of reactive oxygen species induced by AR [7,8]. Therefore, it has become increasingly crucial to recognize AR inhibition as an essential strategy for preventing and attenuating long-term diabetic complications. Thus, in our pursuit of identifying effective treatments for diabetic complications, we have chosen to concentrate on AR inhibitors (ARIs) due to many compelling factors.

According to existing research, most recognized ARIs are classified into four distinct chemical classes: (a) carboxylic acid derivatives, (b) cyclic spiroimides, (c) phenolic derivatives, and (d) phenylsulfonylnitromethane derivatives [9]. Over the years, various carboxylic acid ARIs, such as Alrestatin, Epalrestat (EPR), Lidorestat, Tolrestat, Ponalrestat, Zenarestat, and Zopolrestat, have been synthesized [10] (Fig. 2). However, all these agents exhibit low pKa values, leading to high ionization at physiological blood pH. Additionally, they display low *in vivo* activity and poor tissue penetration. As a result, researchers conducted a series of studies to synthesize new chemotypes of carboxylic acid. Despite developing several ARI agents with promising *in vitro* and *in vivo* efficacy, only EPR has been approved in Japan for treating diabetic neuropathy [11]. The remaining compounds were withdrawn after clinical trials due to their poor pharmacokinetic profile or the emergence of side effects [12].

The resolution to the inadequate pharmacokinetic profile of carboxylic acids was achieved through the emergence of spirohydantoin derivatives [13]. The most extensively investigated compounds of this category are Sorbinil and Fidarestat (Fig. 3). They exhibited a superior pharmacokinetic profile due to their higher pKa values compared to carboxylic acid. Nevertheless, it was discovered that spirohydantoins were associated with grave adverse effects, i.e., hepatic toxicity, cutaneous eruption, and hypersensitivity, rendering them undesirable therapeutic agents [14].

Limiting the adverse effects and improving the permeability of cell membranes are crucial prerequisites in developing novel ARIs. In this regard, innovative ARIs that do not fall under the categories of carboxylic acid or hydantoin derivatives have been investigated. One class comprises spirosuccinimides, including Minalrestat and Ranirestat (as depicted in Fig. 3). Minalrestat has been discontinued due to liver toxicity. In contrast, Ranirestat is currently undergoing phase III clinical trials [15]. Since then, various characteristic derivatives of carboxylic acids and their bioisosteres have been developed; however, the limited number of existing clinical ARIs for preventing diabetic complications underscores the urgent need to discover novel ARIs.

Proficiently identifying a solitary molecule that can target biomolecules or exhibit several antidiabetic effects precisely could offer compelling candidates. In pursuit of this objective, varied scaffolds serving as multifunctional inhibitors of AR have garnered significant interest in managing type-2 Diabetes Mellitus (DM).

In recent years, some researchers have sought to circumvent the toxic effects of established cyclic spirobased agents and the unfavorable pharmacokinetic characteristics of highly ionized carboxylic acids. In pursuit of this goal, they have explored the potential of cyclic imides and other bioisosteres. Many of these bioisosteric substitutions have yielded ARIs that are less ionized and more lipophilic while exhibiting high efficacy *in vivo*. This approach is promising for developing ARIs characterized by enhanced safety and cell membrane permeability, and an optimal ADME profile.

Spirooxindole is an exemplary representative of a heterogeneous group of organic compounds derived from isatin [16]. These compounds possess remarkable biological properties and constitute a significant proportion of pharmaceuticals and biologically active natural products that exhibit all-purpose pharmacological activities [17]. The salient characteristic of spirooxindoles is the presence of diverse heterocyclic motifs attached at the C-3 position of the oxindole ring. This status-unique feature renders them as up-and-coming candidates in drug discovery [18].

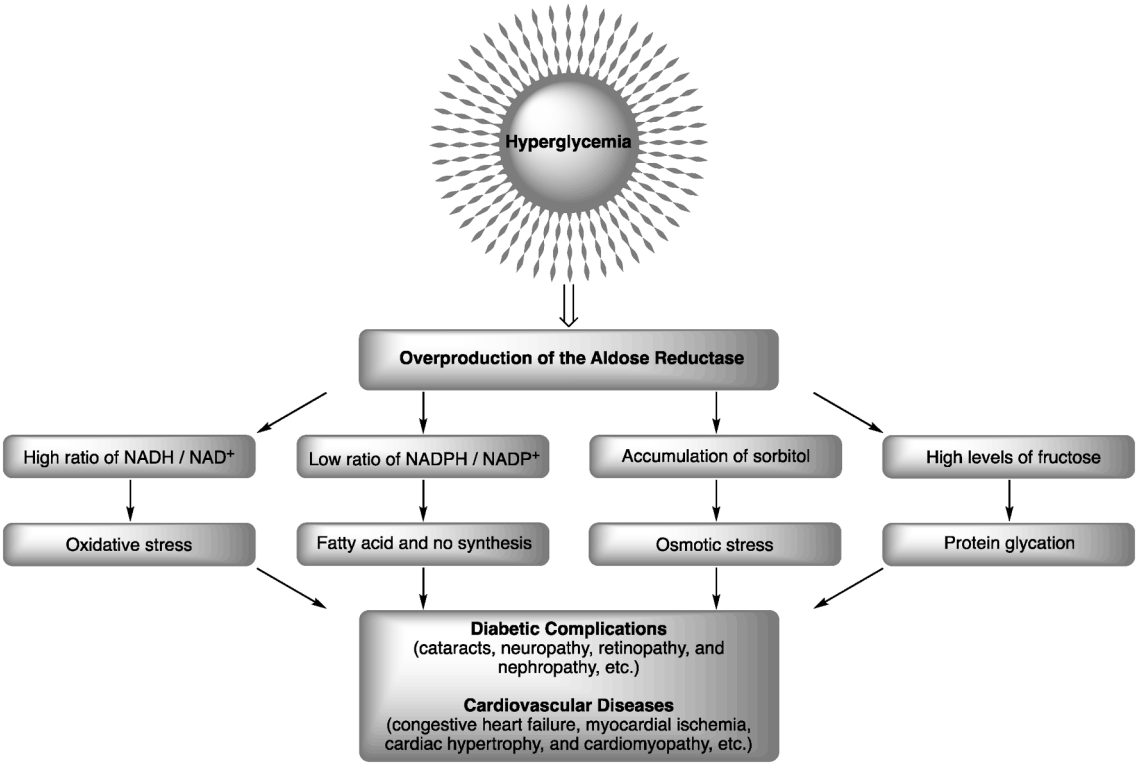

Fig. 1. Diagram illustrating Aldose reductase's (AR) function in the polyol pathway [88].

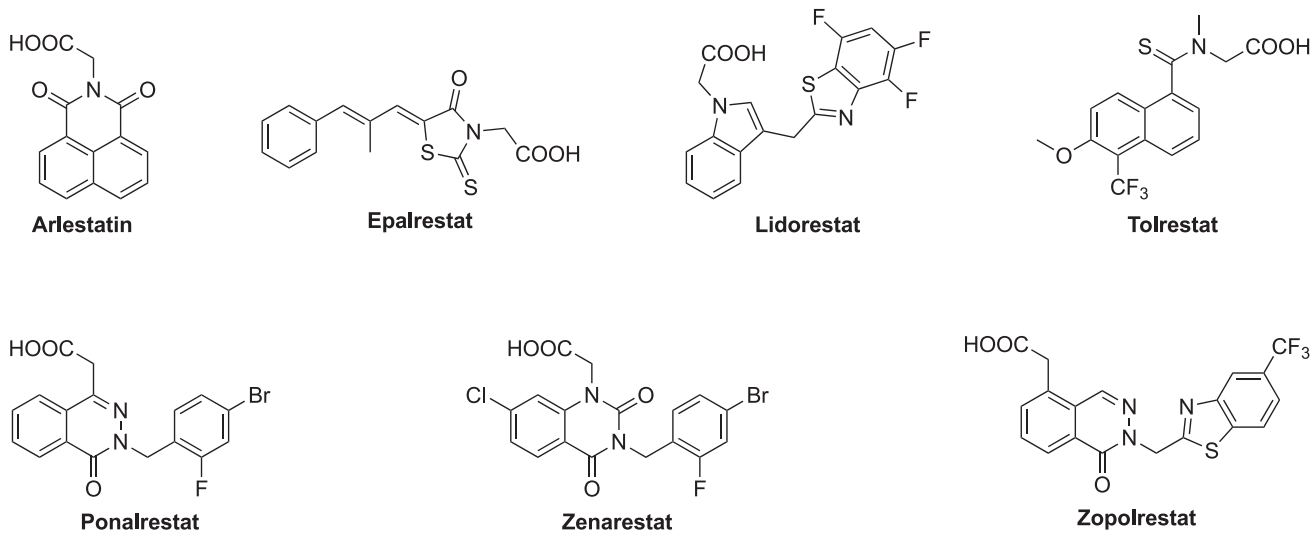

Fig. 2. Structures of some clinically tested carboxylic acid-based Aldose reductase (AR) inhibitors.

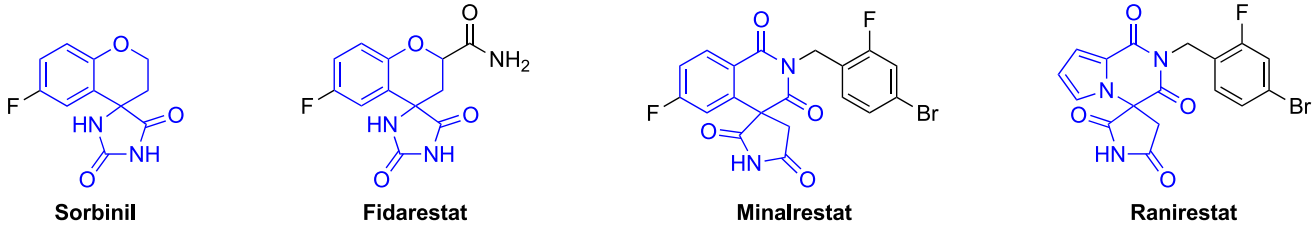

Fig. 3. Aldose reductase (AR) inhibitors developing through clinical trials.

The simultaneous utilization of bioactive macromolecules with complementary pharmacophoric functions or disparate mechanisms of action often manifests synergistic effects [19,20]. Thus, developing structurally innovative inhibitors remains a crucial undertaking in drug discovery. As a continuation of prior work in this area [21–25], the current research delineates a comprehensive investigation into the active catalytic site of AR and the creation of a collection of spiroindoline derivatives that exhibit a preference for binding at AR. In light of this, newly synthesized hybrid spiroindoline oxadiazolyl-based acetate derivatives **6(a-o)** have been devised as promising inhibitors for certain complications.

2. Results and discussions

2.1. Drug design strategy and chemistry

Although ARIs have a variety of chemical structures, they exhibit unique structural characteristics. Research has shown that the minimal

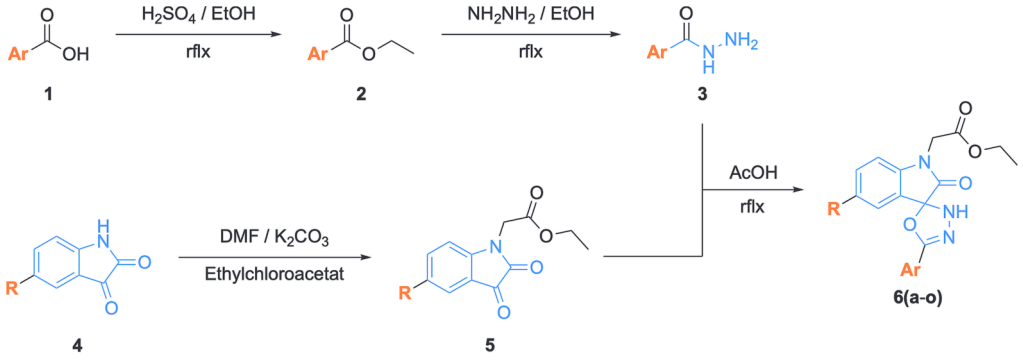

Compounds	R	Ar	Compounds	R	Ar	Compounds	R	Ar
6a	H	4-OCH_3PhCH_2	**6f**	Cl	4-OCH_3PhCH_2	**6k**	NO_2	4-OCH_3PhCH_2
6b	H	Ph	**6g**	Cl	Ph	**6l**	NO_2	Ph
6c	H	Pyridine	**6h**	Cl	Pyridine	**6m**	NO_2	Pyridine
6d	H	4-NO_2Ph	**6i**	Cl	4-NO_2Ph	**6n**	NO_2	4-NO_2Ph
6e	H	4-SO_2NH_2Ph				**6o**	NO_2	4-SO_2NH_2Ph

Scheme 1. Synthetic route targeting spiroindoline oxadiazolyl-based acetate derivatives **6(a-o)**.

pharmacophore requirement for ARIs consists of a polar or ionic group and two hydrophobic aromatic systems joined by a flexible linker [26]. This finding has led to the inclusion of an acidic group in most ARIs, which can strongly interact with key catalytic amino acids, e.g., Trp20, Tyr48, Lys77, His110, and Trp111, and the nicotinamide moiety of $NADP^+$ in the anion-binding pocket through hydrogen bonding [27]. In this direction, based on our preliminary molecular docking search, we aimed to build a capping group to accommodate the AR binding site while also targeting the pocket identified in AR and shaped by these five residues. We envisaged combining a bulky spiroindoline cap group with an acetate moiety and the linker moiety containing an oxadiazole ring. Moreover, we inserted R and Ar groups into this scaffold for their structure–activity relationships (SARs) study (Scheme 1). In addition to their utilization as beneficial medicinal chemistry and drug discovery templates, spirofused scaffolds have the potential to offer various advantages, as evidenced by their increasing prevalence in literature [28,29]. For example, incorporating a spirofused ring could facilitate the development of achiral molecules. Furthermore, the conformational restriction from spiro ring formation may enhance bioavailability and metabolic stability and diminish off-target activities [30]. Therefore, it could confer more favorable physical properties to the structure than molecules featuring numerous flat rings [31]. Moreover, incorporating a spiroring fusion may also represent a valuable approach for augmenting molecular complexity, potentially offering more significant benefits than introducing flat rings [32,33].

From carboxylic acid in ethanol with a catalytic quantity of sulphuric acid, carboxylic acid ethyl esters were made by refluxing for 24 hrs. With the help of hydrazine hydrate and ethanol at 70 °C for 24 hrs, the ester group was changed into a hydrazide. Alkylation of isatin derivatives (**5**) was carried out from isatin derivatives and ethylchloroacetate with K_2CO_3 in DMF at 80 °C for 12 hrs. The final targeted spiroindoline oxadiazolyl-based acetate derivatives **6(a-o)** were synthesized using 4-(hydrazinecarbonyl) benzene and *N*-ethylacetate indoline-2,3-dione compounds in acetic acid for 3 hrs at 100 °C. IR, NMR (^1H and ^{13}C), and Mass spectroscopy were used to identify the prepared compounds. Scheme 1 displays the suggested compounds **6(a-o)**.

According to the ^1H NMR spectra, the N—H proton on the oxadiazol ring and sulphanilamide NH_2 resonance at around 13.10 ppm and 7.60 ppm, respectively, and the =CH proton peaks on the aromatic ring come between 7.00 and 8.50 ppm. The carbonyl group signals on the isatin ring and ester are seen in the ^{13}C NMR spectra at about 160 and 170 ppm. In the infrared spectra of target compounds **6(a-o)**, it was possible to observe the absorptions between 3200 and 3400 cm^{-1} relating to NH and NH_2 stretching peaks for sulphonamide compounds and absorptions in 1550–1700 cm^{-1} from carbonyl moiety stretching. As the literature for the sulphonamide derivatives shows, two peaks are assigned to SO_2 as symmetric and asymmetric stretching [34]. The asymmetric and symmetric stretch peaks appeared around 1350 and 1150 cm^{-1}, respectively. For the nitro derivatives, two peaks are assigned to NO_2 as asymmetric and symmetric stretching, which occur about 1540 and 1350 cm^{-1}, respectively. The synthesized compounds' structures are supported by all of the spectra and elemental analyses.

2.2. Aldose reductase inhibition assay

The inhibitory potential of fourteen novel synthesized spiroindoline oxadiazolyl-based acetate derivatives **6(a-o)** was evaluated *in vitro* for their ability to inhibit AR, an important polyol pathway enzyme especially closely related to diabetic complications. The performed analyses were based on a spectrometric measurement at 340 μM, which is proven to be a reliable method, with NADPH (Sigma N1630, PubChem CID: 5884) as the cofactor and DL-glyceraldehyde as the substrate according to Cerelli's method. The experiments used EPR (Sigma SML0527, PubChem CID: 1549120), a well-known ARI, as a reference inhibitor. Table 1 lists the results, including the inhibitory constants (K_I, μM) and the AR-related corresponding coefficient of determination (R^2).

Table 1
Inhibition data of aldose reductase (AR) with novel synthesized spiroindoline oxadiazolyl-based acetate derivatives **6(a-o)** compared to reference inhibitor Epalrestat.

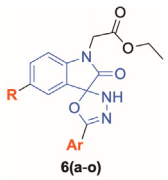

6(a-o)

Compounds			K_I [a] (μM)	R^2
ID	R	Ar		
6a	H	4-OCH_3PhCH_2	0.407 ± 0.022	0.9885
6b	H	Ph	0.442 ± 0.024	0.9880
6c	H	Pyridine	0.615 ± 0.034	0.9875
6d	H	4-NO_2Ph	0.522 ± 0.037	0.9864
6e	H	4-SO_2NH_2Ph	0.397 ± 0.039	0.9874
6f	Cl	4-OCH_3PhCH_2	0.453 ± 0.027	0.9878
6g	Cl	Ph	0.353 ± 0.033	0.9888
6h	Cl	Pyridine	0.409 ± 0.039	0.9886
6i	Cl	4-NO_2Ph	0.811 ± 0.041	0.9896
6k	NO_2	4-OCH_3PhCH_2	0.186 ± 0.020	0.9843
6l	NO_2	Ph	0.344 ± 0.019	0.9870
6m	NO_2	Pyridine	0.662 ± 0.042	0.9860
6n	NO_2	4-NO_2Ph	0.192 ± 0.028	0.9742
6o	NO_2	4-SO_2NH_2Ph	0.532 ± 0.035	0.9859
EPR [b]	–	–	0.841 ± 0.051	0.9893

[a] The analysis outcomes were presented as means of triplicate assays ± SEM.
[b] Epalrestat.

As shown in Table 1, AR inhibitory effects of the synthesized molecules were characterized by the K_I constants ranging from 0.186 ± 0.020 μM for compound **6k** (Figs. 4. and S29) to 0.811 ± 0.041 μM for compound **6i**. The AR inhibition efficacy of all compounds **6(a-o)** markedly exceeded that of the clinically utilized EPR (K_I of 0.841 ± 0.051 μM). Compound **6k** comprises an aryl moiety with a 1-methoxy-4-methylbenzene group added, making it more lipophilic and increasing its interaction with the active site of AR. The derivative **6n**, which has a nitrobenzene group at the aryl moiety and a K_I value of 0.192 ± 0.028 μM, was the subsequent most active derivative, possibly for the same reason. Similarly, with K_I constants of 0.344 ± 0.019 μM and 0.353 ± 0.033 μM, respectively, compound **6l** with a nitro substitute and

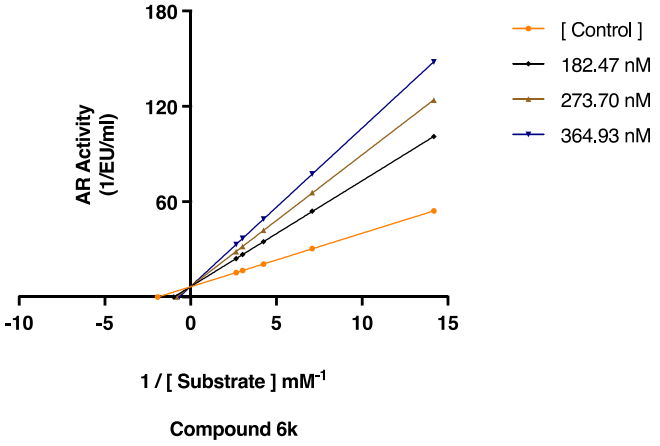

Fig. 4. *In vitro* inhibition effect of compound **6k** against aldose reductase (AR). Lineweaver-Burk plot determined this inhibitor's K_I constant and inhibition type. Different **6k** concentrations were tested for the five levels (0.071, 0.141, 0.235, 0.329, and 0.376 mM) of DL-glyceraldehyde as a substrate to measure AR activity for this aim.

derivative **6g** with a chlorine substitute also have an aryl benzene ring and demonstrate effective inhibition. Furthermore, unsubstituted compounds **6e** and **6a** with bearing benzenesulfonamide and 1-methoxy-4-methylbenzene groups, respectively, showed potent but less inhibition compared to previous (K_Is of 0.397 ± 0.039 μM and 0.407 ± 0.022 μM, respectively). The results reveal that the order of inhibition of these compounds versus AR can be presented as follows: **6k** > **6n** > **6l** > **6g** > **6e** > **6a** > **6h** > **6b** > **6f** > **6d** > **6o** > **6c** > **6m** > **6i**.

In literature, spirocompounds are constituents of a significant portion of pharmaceuticals and biologically active natural products that possess all-round pharmacological activities. Vincristine and Vinblastine represent a class of commercially available anticancer agents that incorporate the spiroindole moiety [35]. Furthermore, the spiroindole-based natural product, Perophoramidine, has been found to exhibit a cytotoxic effect on HMT116 colon carcinoma cells [36]. In this direction, Budovska and colleagues [37] conducted a study wherein they synthesized a series of spiroindoles substituted with trifluoromethylphenylamino and assessed their potential as anticancer agents versus approximately eight cancer cell lines, utilizing cisplatin as a reference drug. They discovered that among the eight cell lines evaluated, cis- and *trans*-diastereoisomers of 2,2′-diamino derivatives with two 3,5-bis(trifluoromethyl)phenylamino functionality showed potent anticancer effects versus five of them. In another study, Rao and co-authors [38] reported on their study that examined a spiroindoline conjugated Calix 4 arene as an anticancer agent versus the MDA-MB-231 cell line. The Cu(II)-complex of compound **L** was found to possess cytotoxic activity versus the MDA-MB-231 cell line, with an IC_{50} of 165 μM. Further investigation revealed that copper facilitated cell death while agent **L** alone remained non-toxic to cancer cells.

Iqbal et al. [39] reported the synthesis of a novel class of spiroimidazolidine-2′,4′-diones substituted with an aryl sulfonyl moiety at various positions. These spiroagents had an inhibitory activity for human recombinant AR with IC_{50} values ranging from 0.56 ± 0.05 μM to 40.15 ± 011 μM. Furthermore, against AR, some of these compounds, **3f** (IC_{50}: 0.56 ± 0.05 μM) and **3g** (IC_{50}: 0.64 ± 0.03 μM), displayed effective inhibition activities compared to reference inhibitors Sorbinil and EPR (IC_{50}s: 0.75 ± 0.02 μM and 0.62 ± 0.04 μM, respectively). In another study, Salem et al. [40] have developed novel AR inhibitors with marked hypoglycemic effects *in vivo*. The study involved the synthesis of two primary categories of compounds. In the first category, the spiroimidazolidine-2,4-dione moiety's C5 was connected to a cyclohexane ring, and in the second category, the same place was filled with a fluorene ring. The authors also rearranged the side chain on the N1 of the spirohydantoin ring to create the appropriate derivatives. **3e** (IC_{50} of 0.37 ± 0.05 μM) exhibited the most potent inhibitory activity in this series compared to Sorbinil with an IC_{50} value of 3.14 ± 0.02 μM. Furthermore, *in vivo* studies indicated an 84.3 % reduction in blood glucose levels.

Da Settimo et al. [41] provided a description of the synthesis and SAR of novel spirohydantoin derivatives. The synthesized thiopyrano [2,3-*b*]pyridin-4(4*H*)-one derivatives were assessed. It was discovered that compounds **3** and **4** in this series displayed potent AR inhibition (IC_{50}s: 0.96 μM and 0.94 μM, respectively) compared to reference inhibitors Tolrestat (IC_{50} of 0.05 μM), Quercetin (IC_{50} of 7.81 μM), and Sorbinil (IC_{50} of 0.65 μM). Notably, compound **3** was topically applied as an eye drop solution *in vivo*, and it exhibited remarkable efficacy in preventing cataract formation in galactosemic rats. In another study, Inoue et al. [42] have published a report detailing synthesizing a new series of dibenzocycloheptanone derivatives. The necessary pharmacophore combinations for AR inhibition were combined to produce these compounds. According to the researchers, the spirosuccinimide ring could interact with residues in the anion-binding site of AR. The cycloheptanone moiety must also have a double bond for the compound to function at its best. On the other hand, the double bond reduction led to a notable decline in AR inhibition. These agents' activities were moderate compared to the Methosorbinil, reference an ARI, with IC_{50} of 0.059 μM. The compound with the highest activity was **11** (spiro{2,8-dihydroxy-5*H*-dibenzo[*a*,*d*]cycloheptene-5,3′-pyrrolidine}-2′,5′-dione) in this series, with an IC_{50} value of 3 μM.

2.3. Structure-activity relationships (SARs)

The examination of the data about inhibition, as presented in Table 1, has brought to the fore specific noteworthy trends in SARs.

As evident from Table 1, the unsubstituted **6a** from the 1-methoxy-4-methylbenzene group derivatives displayed potent inhibitory potency against AR with a K_I value of 0.407 ± 0.022 μM. Introducing a nitro group into position 5 of the indoline scaffold caused a dramatic rise in the affinity to AR (compound **6k** with K_I of 0.186 ± 0.020 μM). In contrast, the activity of chlorine derivative **6f** against AR decreased insignificantly compared to that of **6a**, reaching 0.453 ± 0.027 μM. Similarly, compounds **6l**, **6m**, and **6o** bearing nitro substitutes in the position 5th of the indoline substructure were characterized with a nanomolar range of K_I's versus the AR (0.344 ± 0.019 μM, 0.662 ± 0.042 μM, and 0.532 ± 0.035 μM, respectively). On the other hand, the K_I value of the derivative **6n** (Ar: nitrobenzene), a more potent inhibitor than compounds **6l**, **6m**, and **6o**, towards the AR corresponded to 0.192 ± 0.028 μM, similar to **6k** in this group.

In contrast to the discussed derivatives **6k**, **6l**, and **6n**, unsubstituted spiroindoline oxadiazolyl-based acetates (**6b**, **6c**, **6d**, and **6e**) displayed less inhibition against AR. Although compound **6d** has the same aryl group (nitrobenzene) as **6i** and **6n**, the K_I value against AR was influenced by other substitute patterns, retaining at the level of 0.522 ± 0.037 μM, while chlorine substituted derivative **6i** exerted less potent inhibition towards AR with K_I of 0.811 ± 0.041 μM. It is worth mentioning that the introduction of chlorine group (**6f**, **6g**, and **6h**) at position 5 of the indoline scaffold furnished the derivatives possessing equipotent inhibition against AR with K_I values of 0.453 ± 0.027 μM, 0.353 ± 0.033 μM, and 0.409 ± 0.039 μM, respectively. On the contrary, it was **6i**, which was slightly less sensitive to AR.

Indeed, the inhibitory profile of the chlorine **6g** and nitro **6l** derivatives bearing the benzene ring as an aryl group was very close to that of unsubstituted analog **6a**, and they showed nanomolar range inhibition against AR (K_Is of 0.353 ± 0.033 μM and 0.344 ± 0.019 μM, respectively). Noticeably, replacing the benzene ring with pyridine reduced the inhibition affinity of the corresponding counterparts (**6c**, **6h**, and **6m** with K_Is of 0.615 ± 0.034 μM, 0.409 ± 0.039 μM, and 0.662 ± 0.042 μM, respectively) to AR in question.

2.4. Cytotoxic activity assay

As compound **6k** displayed the best inhibitory activity according to K_I constant results towards AR, it was selected to be evaluated for its cytotoxicity activity versus the normal mouse fibroblast cell line (L929). In addition, the human breast adenocarcinoma cell line (MCF-7) was used to check whether there is an antiproliferative effect of compound

Table 2
Cytotoxic activity and selectivity data of novel synthesized spiroindoline oxadiazolyl-based acetate derivative **6k**, the most potent inhibitor in this series on normal mouse fibroblast (ATCC CCL-1, L929) and human breast adenocarcinoma (ATCC HTB-22, MCF-7) cell lines compared to reference inhibitor Doxorubicin.

Compounds ID	IC_{50}[a] (μM)		Selectivity index[b] (S_I)
	L929	MCF-7	
6k	569.58 ± 0.80	110.87 ± 0.42	5.13
DOX[c]	98.26 ± 0.45	158.49 ± 2.73	0.62

[a] The analysis outcomes were presented as means of triplicate assays ± SEM.
[b] The selectivity index (S_I) for cell line: IC_{50} (L929/MCF-7).
[c] Doxorubicin.

6k on cancer cells. Doxorubicin (DOX) was used as a reference anti-tumor drug. Analysis results were presented as the percentage of cell viability by comparing with the untreated control group in Table 2 and expressed as IC_{50} values, which are the compound concentrations needed to produce a 50 % inhibition of cell growth after 24 hrs incubation.

The results showed that the cytotoxic effect of compound **6k** (IC_{50} of 569.58 ± 0.80 nM) on L929 cells was less than DOX (IC_{50} of 98.26 ± 0.45 nM) in the concentration range studied (25–200 nM), and it demonstrated high safety margins. Additionally, it was determined that compound **6k** (IC_{50} of 110.87 ± 0.42 nM) decreased the viability of MCF-7 cells in the same concentration range compared to DOX (IC_{50} of 158.49 ± 2.73 nM) and was found to show significantly more potent anticancer activity. To evaluate any anticancer activity of a compound, its cytotoxicity against non-cancerous cell lines needs to be determined to calculate the selectivity index (S_I) value. Therefore, compound **6k**'s S_I value was estimated using the following formula: (IC_{50} value for L929 cell line)/(IC_{50} value for MCF-7 cell line). The medicines should ideally be able to kill cancer cells without harming healthy cells [43,44]. In this direction, for the MCF-7 cell line, the S_I value of compound **6k** was determined to be 5.13. This finding indicated that compound **6k** specifically suppressed the proliferation of cancerous cells in contrast to non-cancerous cells.

2.5. In silico study

Several enzyme inhibitors have demonstrated *in vitro* inhibition; however, many of them have been eliminated during clinical trials because of their inadequate pharmacokinetic profile. Therefore, an *in silico* ADME/T approach was primarily employed to evaluate the physicochemical and pharmacokinetic characteristics, lipophilicity, and drug-likeness parameters of all targeted molecules at the initial stages of this study to optimize cost, resources, and labor. The calculated parameters are shown in Tables S1–S4. It was observed that all targeted compounds were in line with drug-likeness parameters, such as the Lipinski (Pfizer) [45], Jorgensen (Melinta) [46], Ghose (Amgen) [47], Veber (GSK) [48], Egan (Pharmacia) [49], and Muegge (Bayer) [50] methods and bioavailability score (Abbot) [51] and was not exhibit similarity with the PAINS [52]. Furthermore, it was noted that concerning 'drug-likeness' descriptors, compound **6k**, which is the most potent inhibitor in this series, exhibited significantly more excellent compatibility than EPR (Figs. 5. and S30).

Molecular docking simulations can be conducted using several methods and settings [53–56]. Selection of a method, adjusting settings, and validation steps are crucial to obtain reliable results [57,58]. Hence, we first performed docking of the native ligand and compared the binding conformation with the already known x-ray crystal structure. The Glide SP method successfully generated active conformation with a RMSD value of 0.34 Å. The same protocol and settings were applied in this series's molecular docking of the most potent inhibitor, **6k** (K_I of 0.186 ± 0.020 μM).

Molecular dynamic (MD) simulations were performed to assess the protein–ligand complex's stability and identify vital interacting residues in a biologically simulated environment [59,60]. The docked pose for compound **6k** was used as initial input, and several parameters were measured during 200 ns of simulation. RMSD values of the Cα backbone (blue) for the complex based on the reference frame backbone were computed to see the effect of the ligand on the conformational stability throughout the simulation (Fig. 6, top panel). Following initial fluctuation, it took 50 ns for the protein–ligand complex to reach equilibrium. The system-maintained stability till the end of the simulation with minor RMSD fluctuations that were within 1 Å. The ligand RMSD plot (red) also showed stability after 25 ns with acceptable fluctuations (~3 Å) (Fig. 6, top panel). Visual inspection of the simulation confirmed that the ligand was not diffused away from the binding pocket. The RMSF value for Cα- atoms was calculated to assess the effect of the ligand on the protein's amino acid residues upon binding. As seen from Fig. 6 (bottom panel), with few exceptions, protein RMSF values are below 2 Å. The residues that compound **6k** is interacting with have much lower RMSF values, meaning the ligand–protein contacts are favorable and stabilize the complex.

The ligand–protein contact graph, shown in Fig. 7, represents vital amino acid residues in which compound **6k** interacts. His110 maintains hydrogen bond and pi-pi interactions, while Trp111 keeps π- π interaction 90 %, 56 %, and 71 % of the time, respectively. Those two amino acid residues are observed in the native ligand-AR crystal structure. In addition to those interactions, a salt bridge is observed between Lys21 and, pi-cation and pi-pi interactions are spotted with Trp20 residue. Another interaction worth mentioning is the hydrogen bond between Asn160 and compound **6k**, which remained for 90 % of the time.

3. Conclusion

In the current work, we describe the design, synthesis, and *in vitro* testing of fourteen spiroindoline oxadiazolyl-based acetate derivatives **6 (a-o)** as inhibitors of various AR-related diabetic complications (cataracts, neuropathy, retinopathy, and nephropathy) and cardiovascular diseases (congestive heart failure, myocardial ischemia, cardiac hypertrophy, and cardiomyopathy) in the polyol pathway. In a broader sense, these compounds exhibited strong inhibition potential versus AR with K_I constants spanning 0.186 ± 0.020–0.662 ± 0.042 μM. However, within the series, two compounds, **6k** (ethyl 2-(5′-(4-methoxybenzyl)-5-nitro-2-oxo-3′*H*-spiro[indoline-3,2′-[1,3,4]oxadiazol]-1-yl)acetate) and **6n** (ethyl 2-(5-nitro-5′-(4-nitrophenyl)-2-oxo-3′*H*-spiro[indoline-3,2′-[1,3,4]oxadiazol]-1-yl)acetate) (K_Is of 0.186 ± 0.020 μM and 0.192 ± 0.028 μM, respectively) were found to be better inhibitors of AR in

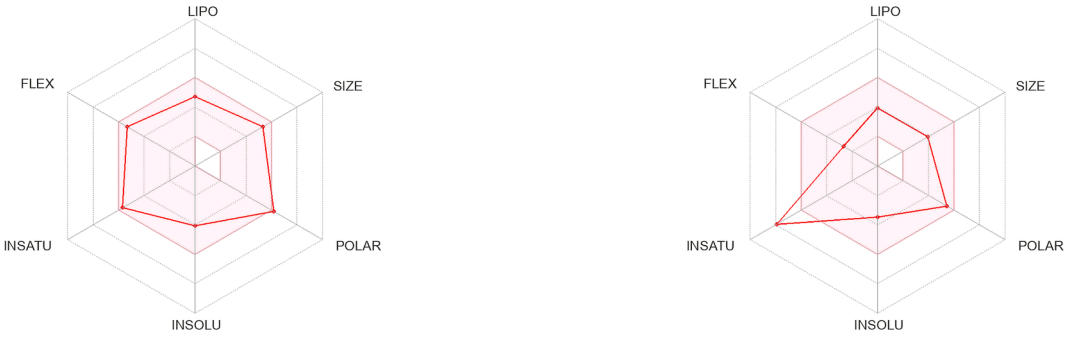

Fig. 5. Diagrams showing 'drug-likeness' descriptors for this series' most potent inhibitor, **6k** (ethyl 2-(5′-(4-methoxybenzyl)-5-nitro-2-oxo-3′H-spiro[indoline-3,2′-[1,3,4]oxadiazol]-1-yl)acetate) (left), and reference inhibitor Epalrestat, a clinically used drug (right). The red-colored zone has been identified as a feasible physicochemical domain to enhance oral bioavailability (LIPO, lipophilicity; SIZE, molecular weight; INSOLU, insolubility; INSATU, saturation; and FLEX, flexibility).

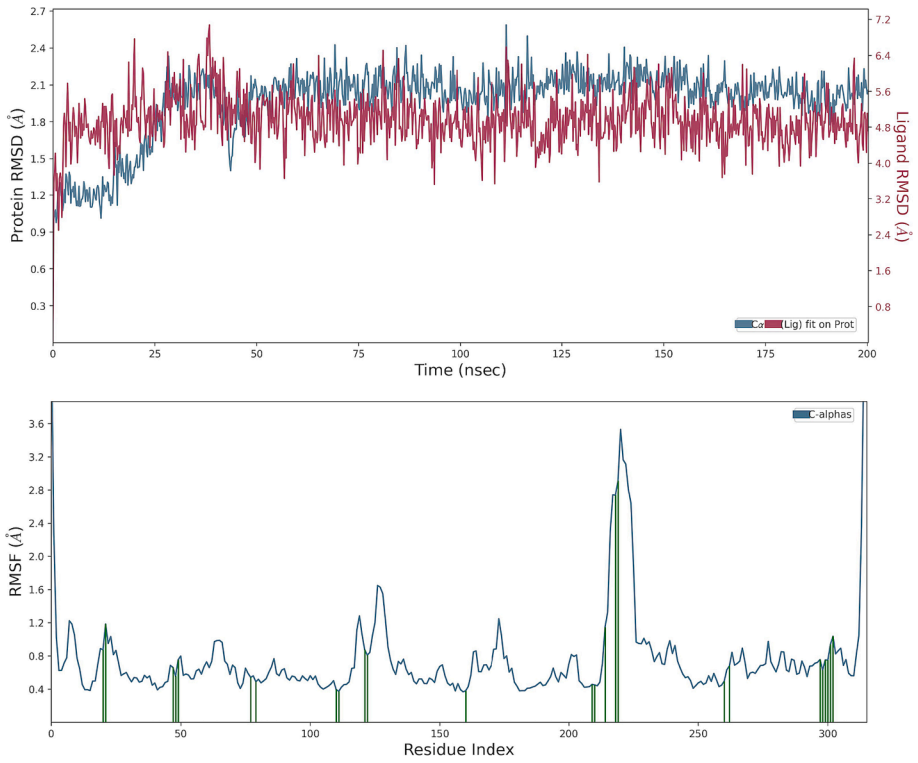

Fig. 6. Aldose reductase enzyme (PDB ID: 4JIR) and compound **6k** (ethyl 2-(5′-(4-methoxybenzyl)-5-nitro-2-oxo-3′H-spiro[indoline-3,2′-[1,3,4]oxadiazol]-1-yl)acetate) RMSD (top) and RMSF (bottom) plots.

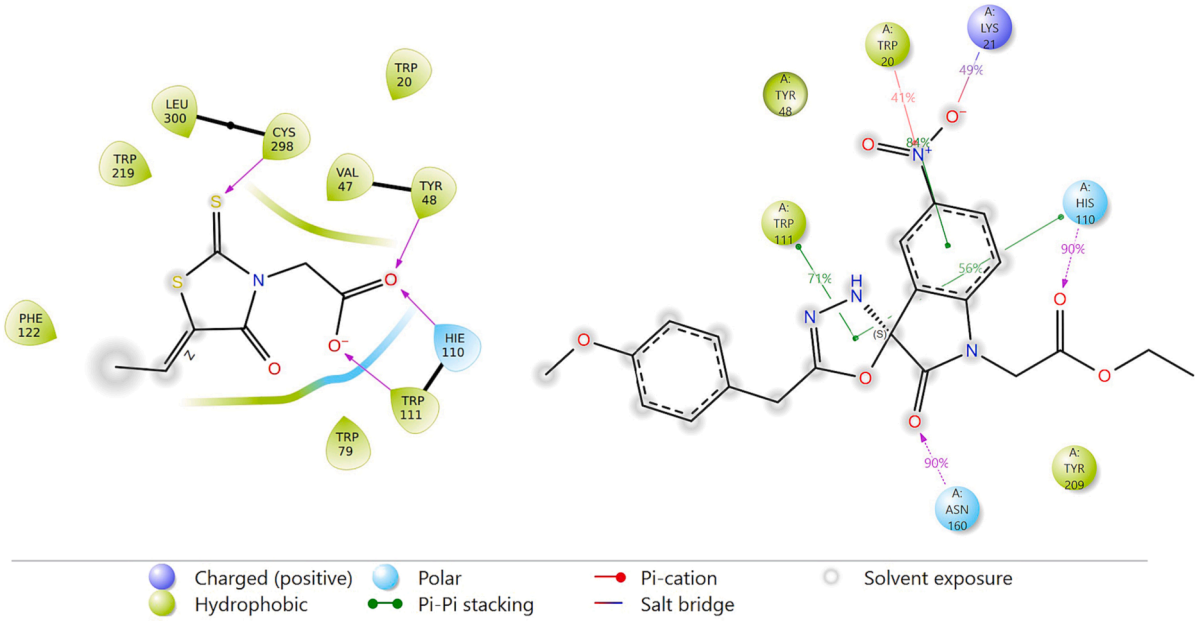

Fig. 7. The 2D ligand interaction diagram of native ligand-AR (PDB ID: 4JIR) crystal structure (left), and ligand contact of compound **6k**-AR for 50 % of 200 ns simulation (right).

comparison to reference drug EPR (K_I: 0.841 ± 0.051 μM) with **6k** as the most potent inhibitor. Also, the most potent AR inhibitor, **6k**, displayed marked inhibitory activity against normal mouse fibroblasts (cell migration and toxicity) and human breast adenocarcinoma cell line (cell cycle and apoptosis) in a dose-dependent manner; L929 (IC_{50} of 569.58 ± 0.80 μM) and MCF-7 (IC_{50} of 110.87 ± 0.42 μM). Namely, **6k** had less cytotoxic effect on L929 cells and reduced the viability of MCF-7 cells more compared to reference drug DOX (IC_{50}s of 98.26 ± 0.45 μM for L929 and 158.49 ± 2.73 μM for MCF-7). Additionally, MD simulations were executed for a duration of 200 ns to forecast the stability of the docked complex and ascertain essential amino acid residues that were interacted with by the **6k**. The current study offers insightful information about the inhibition data of fourteen novel synthesized spiroindoline oxadiazolyl-based acetate derivatives **6(a-o)**, particularly regarding SARs and *in silico* studies. The results demonstrate the potential of these derivatives, which can be effectively utilized in designing innovative

and advanced molecules against diabetic complications and cardiovascular diseases in the DM process.

4. Experimental section

4.1. General procedure for the preparation of the target compounds

A Yanagimoto micro-melting point apparatus determined melting points and was uncorrected. IR spectra were acquired on a SHIMADZU Prestige-21 (200 VCE) spectrometer. ^{1}H- and ^{13}C NMR spectra were acquired at VARIAN Infinity Plus at 300 and 75 Hz, respectively. ^{1}H and ^{13}C chemical shifts are referenced to the internal deuterated solvent. The Mass analysis was carried out with an LC/MS QTOF-9030 spectroscopy. All chemicals were purchased from Alfa Aesar, Merck, and Sigma-Aldrich.

4.1.1. General procedure for preparation of ester derivatives (2)

Carboxylic acid derivatives (**1**) (10 mmol) were refluxed in 50 ml of ethanol for 24 hrs in the presence of 1.0 ml of sulfuric acid as a catalyst. At the end of the reaction, the solvent was evaporated, and the obtained product was washed with cold water and dried. ^{1}H- and ^{13}C NMR checked the purity of the compound, and the compound was used for the next step without further purification.

4.1.2. General procedure for preparation of hydrazide derivatives (3)

Ester derivatives (**2**) (10 mmol) and hydrazine hydrate (25 mmol) in ethanol were refluxed for 24 hrs at 80 °C. At the end of the reaction, the reaction mixture was cooled to room temperature, and the solid was filtered, then washed with water and dried. ^{1}H- and ^{13}C NMR checked the purity of the compound, and the compound was used for the next step without further purification.

4.1.3. General procedure for the synthesis of ethyl 2-(2,3-dioxoindolin-1-yl)acetate derivatives (5)

Indoline-2,3-dione derivatives (**4**) (5 mmol) and ethylchloroacetat (6 mmol) were dissolved in DMF (6 ml), and K_2CO_3 (5 mmol) was added to the mixture. Then, it was stirred at room temperature for 12 hrs. After the reaction, the mixture was poured into ice-cold water and filtered and crystallized in acetone. ^{1}H- and ^{13}C NMR determined the structure.

4.1.4. General procedure for the synthesis of targeted compounds (6a-o)

Hydrazide derivatives (**3**) (1 mmol) and ethyl 2-(2,3-dioxoindolin-1-yl)acetate derivatives (**5**) (1 mmol) in acetic acid were heated for 12 hrs at 105 °C. After the reaction was completed, the reaction mixture was cooled to room temperature and poured into ice-cold water. The solid was filtered, then washed with water and dried. The targeted products were purified by crystallization in acetone-hexane. The prepared compounds in Scheme 1 were characterized by NMR (^{1}H and ^{13}C), IR, and QTOF LC/MS.

4.1.4.1. Ethyl 2-(5′-(4-methoxybenzyl)-2-oxo-3′H-spiro[indoline-3,2′-[1,3,4]oxadiazol]-1-yl)acetate (6a)

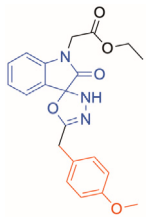

Yield 71 %, m.p. 127 °C; FT-IR (ν, cm^{-1}): 3213 (NH), 2963 (aliphatic C—H) 1739 (ester C═O) and 1686 (amidic C═O); ^{1}H NMR (300 MHz, DMSO-d_6) δ (ppm): 12.24 (s, 1H, –NH), 7,65 (m, 1H, ═CH), 7.43 (d, J = 7.9 Hz, 1H, ═CH), 7.25 (d, J = 8.2 Hz, 2H), 7.16 (d, J = 7.7 Hz, 2H), 6.88 (d, J = 7.9 Hz, 2H), 4.66 (s, 2H, –CH_2), 4.15 (q, J = 7.1 Hz, 2H, –CH_2), 4.06 (s,2H, –CH_2), 3.71 (s, 3H, –CH_3), 1.19 (t, J = 7.2 Hz, 3H, –CH_3); ^{13}C NMR (75 MHz, DMSO-d_6) δ (ppm): 169.5 (ester C═O), 168.1 (amidic C═O), 161.2 (oxadiazole ring C═N), 158.9 (O-Ph), 143.2, 132.3, 132.0, 131.2, 126.9, 124.0, 121.1, 119.7, 114.6, 110.7 (chiral carbon), 62.1 ($CH_2COOCH_2CH_3$), 55.6 (CH_2Ph), 41.5 (OCH_2CH_3), 38.1 (OCH_3), 14.5 (OCH_2CH_3); QTOF LC-MS: (m/z) found (2 M + Na): 813.28, (M + Na): 418,1339; calculated [$C_{21}H_{21}N_3O_5$]: 395.41 [M]$^{+}$.

4.1.4.2. Ethyl 2-(2-oxo-5′-phenyl-3′H-spiro[indoline-3,2′-[1,3,4]oxadiazol]-1-yl)acetate (6b)

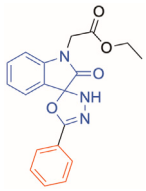

Yield 78 %, m.p. 149 °C; FT-IR (ν, cm^{-1}): 3210 (NH), 2985 (aliphatic C—H) 1740 (ester C═O) and 1705 (amidic C═O); ^{1}H NMR (300 MHz, DMSO-d_6) δ (ppm): 13.67 (s, 1H, –NH), 7.90 (d, J = 5.1 Hz, 2H, ═CH), 7.68 (d, J = 6.2 Hz, 2H, ═CH), 7.61 (d, J = 7.4 Hz, 2H, ═CH), 7.47 (t, J = 8.7, 1H, ═CH), 7.19 (t, J = 9.0, 2H, ═CH), 4.70 (s, 2H, –CH_2), 4.16 (q, J = 7.1, 1H, –CH_2), 1.20 (t, J = 7.1, 3H, –CH_3); ^{13}C NMR (75 MHz, DMSO-d_6) δ (ppm): 168.1 (ester C═O), 164.2 (amidic C═O), 161.8 (oxadiazole ring C═N), 143.3, 130.7, 133.7, 132.5, 132.4, 129.9, 128.1, 124.3, 121.5, 119.6, 111.0 (chiral carbon), 62.1 ($CH_2COOCH_2CH_3$), 41.6 (OCH_2CH_3), 14.6 (OCH_2CH_3); QTOF LC-MS: (m/z) found (2 M + Na): 725.2297, (M + Na): 374.1088; calculated [$C_{19}H_{17}N_3O_4$]: 351.36 [M]$^{+}$.

4.1.4.3. Ethyl 2-(2-oxo-5′-(pyridin-2-yl)-3′H-spiro[indoline-3,2′-[1,3,4]oxadiazol]-1-yl)acetate (6c)

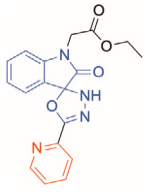

Yield 89 %, m.p. 207 °C; FT-IR (ν, cm^{-1}): 3225 (NH), 2982 (aliphatic C—H) 1740 (ester C═O) and 1702 (amidic C═O); ^{1}H NMR (300 MHz, DMSO-d_6) δ (ppm): 8.72 (d, J = 4.5 Hz, 1H, ═CH), 8.20 (d, J = 7.5 Hz, 1H, ═CH), 8.09 (t, J = 7.6 Hz, 1H, ═CH), 7.77–7.64 (m, 2H, ═CH), 7.45 (t, J = 7.6 Hz, 1H, ═CH), 7.18 (t, J = 7.6 Hz, 2H, ═CH), 4.69 (s, 2H, –CH_2), 4.16 (q, J = 7.1 Hz, 2H, –CH_2), 1.20 (t, J = 7.0 Hz, 3H, –CH_3); ^{13}C NMR (75 MHz, DMSO-d_6) δ (ppm): 168.2 (ester C═O), 161.3 (amidic C═O), 149.7 (oxadiazole ring C═N), 148.7, 143.5, 139.1, 137.9, 132.6, 128.7, 124.2, 123.7, 121.6, 119.7, 110.9 (chiral carbon), 62.1 ($CH_2COOCH_2CH_3$), 41.6 (OCH_2CH_3), 14.6 (OCH_2CH_3); QTOF LC-MS: (m/z) found (2 M + Na): 727.2204, (M + Na): 353.1220, calculated [$C_{18}H_{16}N_4O_4$]: 352.34 [M]$^{+}$.

4.1.4.4. Ethyl 2-(5′-(4-nitrophenyl)-2-oxo-3′H-spiro[indoline-3,2′-[1,3,4]oxadiazol]-1-yl)acetate (6d)

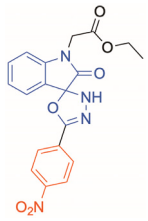

Yield 84 %, m.p. 205 °C; FT-IR (ν, cm^{-1}): 3185 (NH), 2985 (aliphatic C—H) 1736 (ester C═O) and 1708 (amidic C═O), 1524 and 1343 (NO_2); ^1H NMR (300 MHz, DMSO-d_6) δ (ppm): 13.53 (s,1H, –NH), 8.42 (d, J = 7.4 Hz, 2H, ═CH), 8.13 (d, J = 7.1 Hz, 2H, ═CH), 7.65 (t, J = 7.3 Hz, 1H, ═CH), 7.56 (t, J = 7.6 Hz, 1H, ═CH), 7.53 (t, J = 6.2 Hz, 1H, ═CH), 7.27 (d, J = 6.7 Hz, 1H, ═CH), 4.72 (s, 2H, –CH_2), 4.17 (q, J = 7.1, 2H, –CH_2), 1.21 (t, J = 7.1 Hz, 3H, –CH_3); ^{13}C NMR (75 MHz, DMSO-d_6) δ (ppm): 168.1 (ester C═O), 161.8 (amidic C═O), 161.7 (oxadiazole ring C═N), 150.4, 143.5, 138.1, 132.9, 130.2, 129.9, 129.5, 124.8, 124.4, 121.7, 119.4, 111.1 (chiral carbon), 62.2 ($CH_2COOCH_2CH_3$), 41.6 (OCH_2CH_3), 14.6 (OCH_2CH_3); QTOF LC-MS: (m/z) found (M + Na): 419.0930, calculated [$C_{19}H_{16}N_4O_6$]: 396.35 $[M]^+$.

4.1.4.5. Ethyl 2-(2-oxo-5′-(4-sulfamoylphenyl)-3′H-spiro[indoline-3,2′-[1,3,4]oxadiazol]-1-yl)acetate (6e)

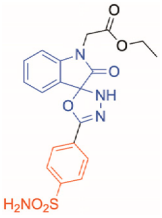

Yield 65 %, m.p. 256 °C; FT-IR (ν, cm^{-1}): 3257 (NH_2), 2975 (aliphatic C—H) 1730 (ester C═O) and 1689 (amidic C═O), 1350 and 1165 (SO_2); ^1H NMR (300 MHz, DMSO-d_6) δ (ppm): 13.62 (s, 1H, –NH), 8.06 (d, J = 8.5 Hz, 2H, ═CH), 8.01 (d, J = 8.5 Hz, 2H, ═CH), 7.67 (d, J = 7.6 Hz, 1H, ═CH), 7.60 (s, 2H, –NH_2), 7.47 (t, J = 7.8 Hz, 1H, ═CH), 7.20 (t, J = 7.2 Hz, 2H, ═CH), 4.70 (s, 2H, –CH_2), 4.16 (q, J = 7.1 Hz, 2H, –CH_2), 1.20 (t, J = 7.1 Hz, 3H, –CH_3); ^{13}C NMR (75 MHz, DMSO-d_6) δ (ppm): 168.1 (ester C═O), 161.7 (amidic C═O), 148.2 (oxadiazole ring C═N), 143.5, 135.4, 132.7, 129.2, 129.1, 127.2, 127.0, 124.4, 121.7, 119.4, 111.1 (chiral carbon), 62.2 ($CH_2COOCH_2CH_3$), 41.6 (OCH_2CH_3), 14.6 (OCH_2CH_3); QTOF LC-MS: (m/z) found (2 M + Na): 686.1482, calculated [$C_{19}H_{18}N_4O_6S$]: 354.34 $[M]^+$.

4.1.4.6. Ethyl 2-(5-chloro-5′-(4-methoxybenzyl)-2-oxo-3′H-spiro[indoline-3,2′-[1,3,4]oxadiazol]-1-yl)acetate (6f)

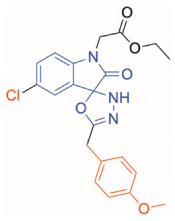

Yield 77 %, m.p. 163 °C; FT-IR (ν, cm^{-1}): 3207 (NH), 2955 (aliphatic C—H) 1745 (ester C═O) and 1689 (amidic C═O); ^1H NMR (300 MHz, DMSO-d_6) δ (ppm): 12.21 (s, 1H, –NH), 7.68 (t, J = 7.2 Hz, 1H, ═CH), 7.48 (d, J = 8.3 Hz, 1H, ═CH), 7.23 (m, 3H, ═CH), 6.88 (d, J = 8.2 Hz, 2H, ═CH), 4.66 (s, 2H, –CH_2), 4.14 (q, J = 7.0 Hz, 2H, –CH_2), 4.03 (s, 2H, –CH_2), 3.71 (s, 3H, –CH_3), 1.19 (t, J = 7.0 Hz, 3H, –CH_3); ^{13}C NMR (75 MHz, DMSO-d_6) δ (ppm): 167.9 (ester C═O), 160.7 (amidic C═O), 158.8 (oxadiazole ring C═N), 141.6, 131.2, 130.8, 130.2, 126.3, 121.2, 120.6, 114.4, 112.2 (chiral carbon), 62.2 ($CH_2COOCH_2CH_3$), 55.5 (CH_2Ph), 41.4 (OCH_2CH_3), 40.8 (OCH_3), 14.5 (OCH_2CH_3); QTOF LC-MS: (m/z) found (2 M + Na): 881.2026, (M + Na): 452,0960, calculated [$C_{21}H_{20}ClN_3O_5$]: 429.86 $[M]^+$.

4.1.4.7. Ethyl 2-(5-chloro-2-oxo-5′-phenyl-3′H-spiro[indoline-3,2′-[1,3,4]oxadiazol]-1-yl)acetate (6g)

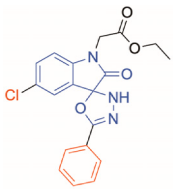

Yield 85 %, m.p. 182 °C; FT-IR (ν, cm^{-1}): 3244 (NH), 2985 (aliphatic C—H) 1741 (ester C═O) and 1708 (amidic C═O); ^1H NMR (300 MHz, DMSO-d_6) δ (ppm): 13.59 (s, 1H, –NH), 7.89 (d, J = 7.5 Hz, 2H, ═CH), 7.68 (d, J = 8.5 Hz, 2H, ═CH), 7.60 (t, J = 7.4 Hz, 3H, ═CH), 7.24 (d, J = 8.5 Hz, 2H, ═CH), 4.70 (s, 2H, –CH_2), 4.15 (q, J = 7.0 Hz, 2H, –CH_2), 1.20 (t, J = 7.1 Hz, 3H, –CH_3); ^{13}C NMR (75 MHz, DMSO-d_6) δ (ppm): 167.9 (ester C═O), 161.5 (amidic C═O), 142.0 (oxadiazole ring C═N), 136.2, 134.0, 133.8, 132.2, 131.8, 130.5, 129.9, 128.6, 128.2, 127.8, 121.3, 121.1, 112.7 (chiral carbon), 62.5 ($CH_2COOCH_2CH_3$), 41.7 (OCH_2CH_3), 14.6 (OCH_2CH_3); QTOF LC-MS: (m/z) found (2 M + Na): 793.1520, (M + Na): 408.0699, calculated [$C_{19}H_{16}ClN_3O_4$]: 385.80 $[M]^+$.

4.1.4.8. Ethyl 2-(5-chloro-2-oxo-5′-(pyridin-2-yl)-3′H-spiro[indoline-3,2′-[1,3,4]oxadiazol]-1-yl)acetate (6h)

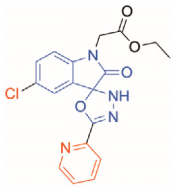

Yield 78 %, m.p. 261 °C; FT-IR (ν, cm^{-1}): 3175 (NH), 2985 (aliphatic C—H) 1747 (ester C═O) and 1705 (amidic C═O); ^1H NMR (300 MHz, DMSO-d_6) δ (ppm): 8.73 (d, J = 6.8 Hz, 1H, ═CH), 8.21 (d, J = 7.7 Hz, 1H, ═CH), 8.10 (t, J = 7.8 Hz, 1H, ═CH), 7.73 (t, J = 6.3 Hz, 1H, ═CH), 7.68 (d, J = 6.7 Hz, 1H, ═CH), 7.50 (d, J = 6.9 Hz, 1H = CH), 7.23 (d, J = 8.4 Hz, 1H, ═CH), 4.70 (s, 2H, –CH_2), 4.16 (q, J = 7.1 Hz, 2H, –CH_2), 1.21 (t, J = 7.0 Hz, 3H, –CH_3); ^{13}C NMR (75 MHz, DMSO-d_6) δ (ppm): 168.0 (ester C═O), 161.5 (amidic C═O), 161.0 (oxadiazole ring C═N), 149.7, 148.5, 142.2, 139.1, 136.8, 131.8, 128.4, 123.8, 121.4, 121.1, 112.6 (chiral carbon), 62.1 ($CH_2COOCH_2CH_3$), 41.7 (OCH_2CH_3), 14.6 (OCH_2CH_3); QTOF LC-MS: (m/z) found (2 M + Na): 793.1520, (M + Na): 408.0695, calculated [$C_{18}H_{15}ClN_4O_4$]: 386.79 $[M]^+$.

4.1.4.9. Ethyl 2-(5-chloro-5′-(4-nitrophenyl)-2-oxo-3′H-spiro[indoline-3,2′-[1,3,4]oxadiazol]-1-yl)acetate (6i)

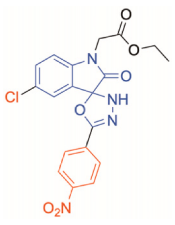

Yield 90 %, m.p. 257 °C; FT-IR (ν, cm^{-1}): 3161 (NH), 2929 (aliphatic C—H) 1736 (ester C═O) and 1689 (amidic C═O), 1515 and 1330 (NO_2); ^{1}H NMR (300 MHz, DMSO-d_6) δ (ppm): 13.63 (s, 1H, –NH), 8.43 (d, J = 8.0 Hz, 2H, ═CH), 8.14 (d, J = 7.0 Hz, 2H, ═CH), 7.67 (s, 1H, ═CH), 7.51 (d, J = 9.0 Hz, 1H, ═CH), 7.22 (d, J = 8.4 Hz, 2H, ═CH), 4.73 (s, 2H, –CH_2), 4.19 (q, J = 6.9, Hz, 2H, –CH_2), 1.23 (t, J = 6.8 Hz, 3H, –CH_3); ^{13}C NMR (75 MHz, DMSO-d_6) δ (ppm): 167.9 (ester C═O), 161.7 (amidic C═O), 161.4 (oxadiazole ring C═N), 145.3, 142.3, 138.8, 132.2, 128.6, 124.9, 124.8, 121.2, 119.2, 116.6, 112.9 (chiral carbon), 62.2 ($CH_2COOCH_2CH_3$), 41.6 (OCH_2CH_3), 14.7 (OCH_2CH_3); QTOF LC-MS: (m/z) found (2 M + Na): 883.1199, (M + Na): 453,0544, calculated [$C_{19}H_{15}ClN_4O_6$]; 430.801 $[M]^+$.

4.1.4.10. Ethyl 2-(5′-(4-methoxybenzyl)-5-nitro-2-oxo-3′H-spiro[indoline-3,2′-[1,3,4]oxadiazol]-1-yl)acetate ***(6k)***

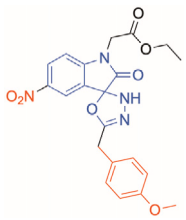

Yield 81 %, m.p. 218 °C; FT-IR (ν, cm^{-1}): 3225 (NH), 2982 (aliphatic C—H) 1733 (ester C═O) and 1698 (amidic C═O), 1514 and 1336 (NO_2); ^{1}H NMR (300 MHz, DMSO-d_6) δ (ppm): 12.27 (s, 1H, –NH), 8,41 (d, J = 9.1 Hz, 1H, ═CH), 8.38 (s, 1H, ═CH), 7.45 (d, J = 8.8 Hz, 1H, ═CH), 7.28 (d, J = 8.3 Hz, 2H, ═CH), 6.90 (d, J = 8.2 Hz, 2H, ═CH), 4.78 (s, 2H, –CH_2), 4.18 (q, J = 7.1 Hz, 2H, –CH_2), 4.05 (s, 2H, –CH_2), 3.73 (s, 3H, –CH_3), 1.22 (t, J = 7.1 Hz, 3H, –CH_3); ^{13}C NMR (75 MHz, DMSO-d_6) δ (ppm): 167.8 (ester C═O), 161.2 (amidic C═O), 158.8 (oxadiazole ring C═N), 147.7, 144.1, 131.3, 131.0, 127.7, 126.6, 120.4, 116.1, 114.5, 114.2, 111.4 (chiral carbon), 62.3 ($CH_2COOCH_2CH_3$), 55.6 (CH_2Ph), 41.9 (OCH_2CH_3), 40.5 (OCH_3), 14.6 (OCH_2CH_3); QTOF LC-MS: (m/z) found (2 M + Na): 903.2519, (M + Na): 463,1204, calculated [$C_{21}H_{20}N_4O_7$]: 440.41 $[M]^+$.

4.1.4.11. Ethyl 2-(5-nitro-2-oxo-5′-phenyl-3′H-spiro[indoline-3,2′-[1,3,4]oxadiazol]-1-yl)acetate ***(6l)***

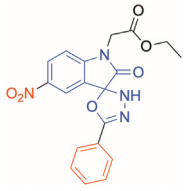

Yield 86 %, m.p. 222 °C; FT-IR (ν, cm^{-1}): 3119 (NH), 3000 (aliphatic C—H) 1739 (ester C═O) and 1692 (amidic C═O), 1517 and 1339 (NO_2); ^{1}H NMR (300 MHz, DMSO-d_6) δ (ppm): 13.44 (s, 1H, –NH), 8.37 (d, J = 8.8 Hz, 1H, ═CH), 8.32 (s, 1H, ═CH), 7.91 (d, J = 7.5 Hz, 2H, ═CH), 7.70 (t, J = 7.2 Hz, 1H, ═CH), 7.61 (t, J = 7.8 Hz, 2H, ═CH), 7.48 (d, J = 9.4 Hz, 1H, ═CH), 4.84 (s, 2H, –CH_2), 4.18 (q, J = 7.1, 2H, –CH_2), 1.21 (t, J = 7.1 Hz, 3H, –CH_3); ^{13}C NMR (75 MHz, DMSO-d_6) δ (ppm): 167.8 (ester C═O), 163.9 (amidic C═O), 161.9 (oxadiazole ring C═N), 147.8, 144.2, 135.3, 133.9, 132.1, 129.9, 129.4, 128.5, 128.3, 128.1, 120.3, 116.3, 111.7 (chiral carbon), 62.3 ($CH_2COOCH_2CH_3$), 42.0 (OCH_2CH_3), 14.6 (OCH_2CH_3); QTOF LC-MS: (m/z) found (2 M + Na): 815.2025, (M + Na): 419,0940, calculated [$C_{19}H_{16}N_4O_6$]: 396.36 $[M]^+$.

4.1.4.12. Ethyl 2-(5-nitro-2-oxo-5′-(pyridin-2-yl)-3′H-spiro[indoline-3,2′-[1,3,4]oxadiazol]-1-yl)acetate ***(6m)***

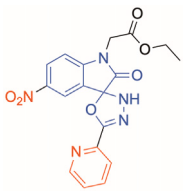

Yield 75 %, m.p. 272 °C; FT-IR (ν, cm^{-1}): 3225 (NH), 2925 (aliphatic C—H) 1723 (ester C═O) and 1698 (amidic C═O), 1483 and 1330 (NO_2); ^{1}H NMR (300 MHz, DMSO-d_6) δ (ppm): 8.77 (s, 1H, ═CH), 8.39 (d, J = 9.1 Hz, 2H, ═CH), 8.24 (d, J = 7.7 Hz, 1H, ═CH), 8.13 (t, J = 7.8 Hz, 1H, ═CH), 7.77 (t, J = 7.1 Hz, 1H, ═CH), 7.49 (d, J = 8.7 Hz, 1H, ═CH), 4.84 (s, 2H, –CH_2), 4.20 (q, J = 7.3 Hz, 2H, –CH_2), 1.24 (t, J = 7.1 Hz, 3H, –CH_3); ^{13}C NMR (75 MHz, DMSO-d_6) δ (ppm): 167.8 (ester C═O), 162.5 (amidic C═O), 161.7 (oxadiazole ring C═N), 150.5, 148.1, 144.3, 137.7, 130.8, 130.1, 130.0, 128.4, 124.8, 120.1, 116.5, 111.8 (chiral carbon), 62.3 ($CH_2COOCH_2CH_3$), 41.4 (OCH_2CH_3), 14.0 (OCH_2CH_3); QTOF LC-MS: (m/z) found (2 M + Na): 817.1909, (M + Na): 420,0892, calculated [$C_{18}H_{15}N_5O_6$]: 397.35 $[M]^+$.

4.1.4.13. Ethyl 2-(5-nitro-5′-(4-nitrophenyl)-2-oxo-3′H-spiro[indoline-3,2′-[1,3,4]oxadiazol]-1-yl)acetate ***(6n)***

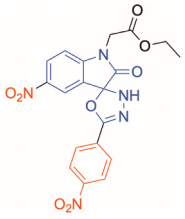

Yield 82 %, m.p. 238 °C; FT-IR (ν, cm^{-1}): 3203 (NH), 2985 (aliphatic C—H) 1698 (ester C═O) and 1599 (amidic C═O), 1525 and 1348 (NO_2); ^{1}H NMR (300 MHz, DMSO-d_6) δ (ppm): 13.41 (s, 1H, –NH), 8.43 (d, J = 7.4 Hz, 3H, ═CH), 8.33 (s, 1H, ═CH), 8.15 (d, J = 8.7 Hz, 2H, ═CH), 7.50 (d, J = 9.1 Hz, 1H, ═CH), 4.84 (s, 2H, –CH_2), 4.20 (q, J = 7.1 Hz, 3H), –CH_2), 1.26 (t, J = 7.6 Hz, 3H, –CH_3); ^{13}C NMR (75 MHz, DMSO-d_6) δ (ppm): 168.8 (ester C═O), 161.7 (amidic C═O), 150.5 (oxadiazole ring C═N), 148.1, 144.3, 137.7, 130.5, 130.1, 128.4, 124.8, 124.4, 120.1, 116.5, 111.8 (chiral carbon), 62.3 ($CH_2COOCH_2CH_3$), 42.0 (OCH_2CH_3), 14.6 (OCH_2CH_3); QTOF LC-MS: (m/z) found (2 M + Na): 905.1686, (M + Na): 464,0786, calculated [$C_{19}H_{15}N_5O_8$]: 441.36 $[M]^+$.

4.1.4.14. Ethyl 2-(5-nitro-2-oxo-5′-(4-sulfamoylphenyl)-3′H-spiro[indoline-3,2′-[1,3,4]oxadiazol]-1-yl)acetate ***(6o)***

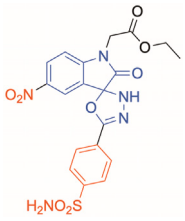

Yield 87 %, m.p. 268 °C; FT-IR (ν, cm^{-1}): 3278 (NH_2), 2957 (aliphatic C—H) 1730 (ester C═O) and 1680 (amidic C═O), 1533 and 1350 (NO_2), 1345 and 1156 (SO_2); ^{1}H NMR (300 MHz, DMSO-d_6) δ (ppm): 13.63 (s, 1H, –NH), 8.53 (s, 1H, ═CH), 8.38 (d, J = 8.8 Hz, 1H, ═CH), 8.09–8.08 (m, 4H, ═CH), 7.51 (s, 2H, –NH_2), 7.41 (d, J = 9.2 Hz, 1H, ═CH), 4.81 (s, 2H, –CH_2), 4.24 (d, J = 7.1 Hz, 1H, –CH_2), 1.30 (t, J = 7.1 Hz, 3H, –CH_3); ^{13}C NMR (75 MHz, DMSO-d_6) δ (ppm): 167.8 (ester C═O), 161.8 (amidic C═O), 148.4 (oxadiazole ring C═N), 148.0,

144.3, 135.0, 129.3, 128.3, 127.0, 120.2, 116.5, 111.7 (chiral carbon), 62.3 ($CH_2COOCH_2CH_3$), 42.0 (OCH_2CH_3), 14.7 (OCH_2CH_3); QTOF LC-MS: (*m/z*) found (2 M + Na): 973.1434, (M + Na): 498,0660, calculated [$C_{19}H_{17}N_5O_8S$]: 475.43 $[M]^+$.

4.2. Biological study

4.2.1. In vitro Aldose reductase inhibition assay

Dimethyl sulfoxide (Sigma D8418, DMSO, PubChem CID: 679) was utilized to prepare solutions of the fourteen-novel synthesized spiroindoline oxadiazolyl-based acetate derivatives **6(a-o)** and EPR at an initial concentration of 1 mg/ml. The proportion of DMSO in the ultimate reaction mixture was roughly 1 %. In keeping with prior research endeavors, kinetic examinations were conducted utilizing Cerelli's method [61,62] with five distinct substrate (DL-glyceraldehyde, Sigma G5001, PubChem CID: 79014) levels (0.071, 0.141, 0.235, 0.329, and 0.376 mM) and varying compound concentrations at 340 nm spectrophotometrically to examine these spiroindolines' *in vitro* inhibitory mechanisms against AR. In this direction, the samples were subjected to three measurements. As in our prior studies [63], Michaelis-Menten plots [64,65] and Lineweaver-Burk curves [66,67] were generated for all compounds **6(a-o)**. K_I constants and their inhibition types were determined based on the obtained data to be competitive and non-competitive.

4.2.2. In vitro cytotoxic activity assay

First, the L929 (ATCC CCL-1) and MCF-7 (ATCC HTB-22) cell lines obtained from ATCC and stored in a cryotube at –80 °C were thawed by incubating in a 37 °C water bath. Later, in DMEM containing 10 % FBS and 1 % penicillin–streptomycin, dissolved cells were transferred to a T75 cm^2 plate. After 48 hrs, these cells were seeded in a 96-well plate that counted at 5×10^3 cells/well. After 24 hrs, L929 and MCF-7 cell lines were exposed to different concentrations (25, 50, 100, 150, and 200 μM) of DOX, a clinically used drug, as a reference control and the most potent inhibitor, **6k** against AR. After 24 hrs of incubation, the MTT method [68,69] was applied using prior protocols [70–72]. Afterward, measurements were taken with a BioTek Epoch Microplate Spectrophotometer (Santa Clara, California, USA) at 570 nm absorbance. The final step was to compare cell viability rates to control wells.

4.3. In silico study

4.3.1. ADME/T study

QikProp tool of the Schrödinger's [73,74] and SwissADME platform [75,76] were together used to predict ADME/T parameters [77,78] such as physicochemical and pharmacokinetic properties, lipophilicity, drug-likeness descriptors, and medicinal chemistry pattern recognition methods for all targeted compounds. As a reference inhibitor, ADME/T studies were carried out by EPR, a clinically used drug.

4.3.2. Molecular docking study

Crystal structure of AR complexed with native ligand (2-{5-[(*E*)-2-methyl-3-phenyl-prop-2-enylidene]-4-oxidanylidene-2-sulfanylidene-1,3-thiazolidin-3-yl}ethanoic acid) was obtained from Protein Data Bank (PDB ID: 4JIR) [79] and prepared using Schrödinger's [80] Protein Preparation Wizard module [81]. In this protocol, missing hydrogens were added, bond orders were assigned, and all water molecules and heteroatoms were deleted except the native ligand [82]. After the optimization step addressing overlapping hydrogens, a restrained minimization was applied using the OPLS4 force field [83]. Before molecular docking, the ligand was also prepared to generate all possible 3D conformations and states at physiological pH conditions via the LigPrep module [84]. The Glide SP method was used for molecular docking [85,86].

4.3.3. Molecular dynamics study

MD simulations were conducted utilizing Desmond implemented in the Schrödinger software package [87]. The system builder panel was first used to prepare the input system. The simple point-charge (SPC) explicit water model was used to build an orthorhombic simulation box with Periodic Boundary Conditions (PBC). The system was neutralized with sodium ions, and a 0.15 M concentration of NaCl was used to mimic physiological conditions. Ion and salt placement were excluded within 20 Å of the ligand. MD was carried out for 200 ns following system relaxation with an isobaric NPT ensemble. 200 ps was used as the recording interval, which produced roughly 1000 frames. The trajectories were evaluated, and all plots were depicted using the simulation interaction diagram (SID) tool.

4.4. Statistical study

The Mac version of GraphPad Prism V9 (La Jolla, California, USA) was used to analyze the data and make the graphs. The Windows version of SigmaPlot V12 (San Jose, California, USA) was utilized to determine the inhibition constants. The extra sum-of-squares, *F* test, and the AIC methods were used to compare the two data sets statistically. The analysis outcomes were presented using the format mean ± standard error of the mean in a 95 % confidence interval when the p-value < 0.05, statistical significance was considered.

CRediT authorship contribution statement

Özcan Güleç: Formal analysis, Investigation, Validation. **Cüneyt Türkeş:** Conceptualization, Formal analysis, Investigation, Methodology, Validation, Writing – original draft, Writing – review & editing. **Mustafa Arslan:** Conceptualization, Formal analysis, Investigation, Methodology, Validation, Writing – original draft, Writing – review & editing. **Yeliz Demir:** Formal analysis, Investigation, Validation. **Busra Dincer:** Formal analysis, Investigation, Validation, Writing – original draft. **Abdulilah Ece:** Formal analysis, Investigation, Software, Validation, Writing – original draft. **Ömer İrfan Küfrevioğlu:** . **Şükrü Beydemir:** Conceptualization, Funding acquisition, Methodology.

Declaration of competing interest

The authors declare that they have no known competing financial interests or personal relationships that could have appeared to influence the work reported in this paper.

Data Availability

The data that support the findings of this study are available from the corresponding author upon reasonable request.

Acknowledgement

Author Özcan GÜLEÇ is a 100/2000 The Council of Higher Education (CoHE) Ph.D. Scholar in the Organic Smart and Innovative Materials Subsection. This work was supported by the Research Fund of Anadolu University (grant number 2102S003). We thank to Sakarya University, Research, Development, and Application Center (SARGEM) for the analysis of the mass spectra of the compounds.

Appendix A. Supplementary data

Supplementary data to this article can be found online at https://doi.org/10.1016/j.bioorg.2024.107221.

References

[1] J. Wu, X. Li, W. Wan, Q. Yang, W. Ma, D. Chen, J. Hu, C.Y.O. Chen, X. Wei, Gigantol from Dendrobium chrysotoxum Lindl. binds and inhibits aldose reductase gene to exert its anti-cataract activity: An in vitro mechanistic study, J. Ethnopharmacol. 198 (2017) 255–261, https://doi.org/10.1016/j.jep.2017.01.026.

[2] S. Thakur, S.K. Gupta, V. Ali, P. Singh, M. Verma, Aldose Reductase: a cause and a potential target for the treatment of diabetic complications, Arch. Pharmacal Res. 44 (2021) 655–667, https://doi.org/10.1007/s12272-021-01343-5.

[3] M. Benlarbi-Ben Khedher, K. Hajri, A. Dellaa, B. Baccouche, I. Hammoum, N. Boudhrioua-Mihoubi, W. Dhifi, R. Ben Chaouacha-Chekir, Astaxanthin inhibits aldose reductase activity in Psammomys obesus, a model of type 2 diabetes and diabetic retinopathy, Food Sci. Nutr. 7 (2019) 3979–3985, https://doi.org/10.1002/fsn3.1259.

[4] J. He, H.-X. Gao, N. Yang, X.-D. Zhu, R.-B. Sun, Y. Xie, C.-H. Zeng, J.-W. Zhang, J.-K. Wang, F. Ding, J.-Y. Aa, G.-J. Wang, The aldose reductase inhibitor epalrestat exerts nephritic protection on diabetic nephropathy in db/db mice through metabolic modulation, Acta Pharmacol. Sin. 40 (2019) 86–97, https://doi.org/10.1038/s41401-018-0043-5.

[5] W.H. Tang, K.A. Martin, J. Hwa, Aldose reductase, oxidative stress, and diabetic mellitus, Front. Pharmacol. 3 (2012) 87, https://doi.org/10.3389/fphar.2012.00087.

[6] Z. Huang, Q. Hong, X. Zhang, W. Xiao, L. Wang, S. Cui, Z. Feng, Y. Lv, G. Cai, X. Chen, D. Wu, Aldose reductase mediates endothelial cell dysfunction induced by high uric acid concentrations, Cell Commun. Sign. 15 (2017) 3, https://doi.org/10.1186/s12964-016-0158-6.

[7] Y.C. Hwang, S. Sato, J.-Y. Tsai, S. Yan, S. Bakr, H. Zhang, P.J. Oates, R. Ramasamy, Aldose reductase activation is a key component of myocardial response to ischemia, FASEB J. 16 (2002) 1–22, https://doi.org/10.1096/fj.01-0368fje.

[8] R. Perfetti, G. Yepuri, N.A. Quadri, A.F. Ghannam, R. Ramasamy, S. Shendelman, 1080-P: addressing the safety challenges of aldose reductase inhibition: development of AT-001 for diabetic cardiomyopathy, a potent and selective next generation aldose reductase inhibitor, Diabetes 69 (2020), https://doi.org/10.2337/db20-1080-P.

[9] J.Á. de la Fuente, S. Manzanaroa, Aldose reductase inhibitors from natural sources, Nat. Prod. Rep. 20 (2003) 243–251, https://doi.org/10.1039/b204709h.

[10] R. Maccari, R. Ottanà, Targeting aldose reductase for the treatment of diabetes complications and inflammatory diseases: new insights and future directions, J. Med. Chem. 58 (2015) 2047–2067, https://doi.org/10.1021/jm500907a.

[11] B.-B. Yang, Z.-W. Hong, Z. Zhang, W. Yu, T. Song, L.-L. Zhu, H.-S. Jiang, G.-T. Chen, Y. Chen, Y.-T. Dai, Epalrestat, an aldose reductase inhibitor, restores erectile function in streptozocin-induced diabetic rats, Int. J. Impotence Res. 31 (2019) 97–104, https://doi.org/10.1038/s41443-018-0075-x.

[12] Y. Hamada, J. Nakamura, Clinical potential of aldose reductase inhibitors in diabetic neuropathy, Treat. Endocrinol. 3 (2004) 245–255, https://doi.org/10.2165/00024677-200403040-00006.

[13] X. Hao, X. Qin, X. Zhang, B. Ma, G. Qi, T. Yu, Z. Han, C. Zhu, Identification of quinoxalin-2(1H)-one derivatives as a novel class of multifunctional aldose reductase inhibitors, Future Med. Chem. 11 (2019) 2989–3004, https://doi.org/10.4155/fmc-2019-0194.

[14] M. Kumar, S. Choudhary, P.K. Singh, O. Silakari, Addressing selectivity issues of aldose reductase 2 inhibitors for the management of diabetic complications, Future Med. Chem. 12 (2020) 1327–1358, https://doi.org/10.4155/fmc-2020-0032.

[15] N. Giannoukakis, Ranirestat as a therapeutic aldose reductase inhibitor for diabetic complications, Expert Opin. Invest. Drugs 17 (2008) 575–581, https://doi.org/10.1517/13543784.17.4.575.

[16] J.J. Badillo, N.V. Hanhan, A.K. Franz, Enantioselective synthesis of substituted oxindoles and spirooxindoles with applications in drug discovery, Curr. Opin. Drug Discovery Dev. 13 (2010) 758–776.

[17] D. Cheng, Y. Ishihara, B. Tan, C.F. Barbas III, Organocatalytic Asymmetric Assembly Reactions: Synthesis of Spirooxindoles via Organocascade Strategies, ACS Catalysis 4 (2014) 743–762, https://doi.org/10.1021/cs401172r.

[18] D. Bora, A. Kaushal, N. Shankaraiah, Anticancer potential of spirocompounds in medicinal chemistry: A pentennial expedition, Eur. J. Med. Chem. 215 (2021) 113263, https://doi.org/10.1016/j.ejmech.2021.113263.

[19] R. Romagnoli, P.G. Baraldi, M.D. Carrion, O. Cruz-Lopez, C.L. Cara, J. Balzarini, E. Hamel, A. Canella, E. Fabbri, R. Gambari, G. Basso, G. Viola, Hybrid α-bromoacryloylamido chalcones. Design, synthesis and biological evaluation, Bioorg. Med. Chem. Lett. 19 (2009) 2022–2028, https://doi.org/10.1016/j.bmcl.2009.02.038.

[20] V.R. Solomon, C. Hu, H. Lee, Hybrid pharmacophore design and synthesis of isatin–benzothiazole analogs for their anti-breast cancer activity, Bioorg. Med. Chem. 17 (2009) 7585–7592, https://doi.org/10.1016/j.bmc.2009.08.068.

[21] G. Yapar, H. Esra Duran, N. Lolak, S. Akocak, C. Türkeş, M. Durgun, M. Işık, Ş. Beydemir, Biological effects of bis-hydrazone compounds bearing isovanillin moiety on the aldose reductase, Bioorg. Chem. 117 (2021) 105473, https://doi.org/10.1016/j.bioorg.2021.105473.

[22] F.S. Tokalı, Y. Demir, İ.H. Demircioğlu, C. Türkeş, E. Kalay, K. Şendil, Ş. Beydemir, Synthesis, biological evaluation, and in silico study of novel library sulfonates containing quinazolin-4(3H)-one derivatives as potential aldose reductase inhibitors, Drug Dev. Res. 83 (2022) 586–604, https://doi.org/10.1002/ddr.21887.

[23] M.D. Altıntop, Y. Demir, C. Türkeş, R.B. Öztürk, Z. Cantürk, Ş. Beydemir, A. Özdemir, A new series of hydrazones as small-molecule aldose reductase inhibitors, Arch. Pharm. (Weinheim, Ger.), 356 (2023) 2200570, https://doi.org/10.1002/ardp.202200570.

[24] F.S. Tokalı, Y. Demir, C. Türkeş, B. Dinçer, Ş. Beydemir, Novel acetic acid derivatives containing quinazolin-4(3H)-one ring: Synthesis, in vitro, and in silico evaluation of potent aldose reductase inhibitors, Drug Dev. Res. 84 (2023) 275–295, https://doi.org/10.1002/ddr.22031.

[25] Y. Demir, F.S. Tokalı, E. Kalay, C. Türkeş, P. Tokalı, O.N. Aslan, K. Şendil, Ş. Beydemir, Synthesis and characterization of novel acyl hydrazones derived from vanillin as potential aldose reductase inhibitors, Mol. Diversity 27 (2023) 1713–1733, https://doi.org/10.1007/s11030-022-10526-1.

[26] M. Schlitzer, L. Rodriguez, P.F. Kador, Synthesis of potential aldose reductase inhibitors based on minimal pharmacophore requirements, J. Pharm. Pharmacol. 53 (2010) 831–839, https://doi.org/10.1211/0022357011776180.

[27] C. Koch, A. Heine, G. Klebe, Ligand-induced fit affects binding modes and provokes changes in crystal packing of aldose reductase, Biochim. Biophys. Acta, General Sub. 1810 (2011) 879–887, https://doi.org/10.1016/j.bbagen.2011.06.001.

[28] Y.-J. Zheng, C.M. Tice, The utilization of spirocyclic scaffolds in novel drug discovery, Expert Opin. Drug Discovery 11 (2016) 831–834, https://doi.org/10.1080/17460441.2016.1195367.

[29] M. Benabdallah, O. Talhi, F. Nouali, N. Choukchou-Braham, K. Bachari, A. Silva, Advances in spirocyclic hybrids: chemistry and medicinal actions, Curr. Med. Chem. 25 (2018) 3748–3767, https://doi.org/10.2174/0929867325666180309124821.

[30] Y. Zheng, C.M. Tice, S.B. Singh, The use of spirocyclic scaffolds in drug discovery, Bioorg. Med. Chem. Lett. 24 (2014) 3673–3682, https://doi.org/10.1016/j.bmcl.2014.06.081.

[31] M. Aldeghi, S. Malhotra, D.L. Selwood, A.W.E. Chan, Two- and three-dimensional rings in drugs, Chem. Biol. Drug Des. 83 (2014) 450–461, https://doi.org/10.1111/cbdd.12260.

[32] F. Lovering, J. Bikker, C. Humblet, Escape from flatland: increasing saturation as an approach to improving clinical success, J. Med. Chem. 52 (2009) 6752–6756, https://doi.org/10.1021/jm901241e.

[33] F. Lovering, Escape from Flatland 2: complexity and promiscuity, Med. Chem. Comm. 4 (2013) 515–519, https://doi.org/10.1039/C2MD20347B.

[34] E. Şen, Z. Alım, H. Duran, M.M. İşgör, Ş. Beydemir, R. Kasımoğulları, S. Ok, Inhibitory effect of novel pyrazole carboxamide derivatives on human carbonic anhydrase enzyme, J. Enzyme Inhib. Med. Chem. 28 (2013) 328–336, https://doi.org/10.3109/14756366.2011.651465.

[35] C.-T. Lee, Y.-W. Huang, C.-H. Yang, K.-S. Huang, Drug delivery systems and combination therapy by using vinca alkaloids, Curr. Top. Med. Chem. 15 (2015) 1491–1500, https://doi.org/10.2174/1568026615666150414120547.

[36] H. Wu, F. Xue, X. Xiao, Y. Qin, Total synthesis of (+)-perophoramidine and determination of the absolute configuration, J. Am. Chem. Soc. 132 (2010) 14052–14054, https://doi.org/10.1021/ja1070043.

[37] M. Budovská, M. Baláž, R. Mezencev, V. Tischlerová, M. Zigová, J. Mojžiš, Design, synthesis and anticancer activity of trifluoromethylphenylamino substituted spiroindoles, J. Fluorine Chem. 216 (2018) 24–32, https://doi.org/10.1016/j.jfluchem.2018.09.011.

[38] R. Nag, S. Polepalli, M. Althaf Hussain, C.P. Rao, Ratiometric Cu2+ binding, cell imaging, mitochondrial targeting, and anticancer activity with nanomolar IC50 by spiro-indoline-conjugated calix[4]arene, ACS Omega 4 (2019) 13231–13240, https://doi.org/10.1021/acsomega.9b01402.

[39] Z. Iqbal, G. Morahan, M. Arooj, A.N. Sobolev, S. Hameed, Synthesis of new arylsulfonylspiroimidazolidine-2',4'-diones and study of their effect on stimulation of insulin release from MIN6 cell line, inhibition of human aldose reductase, sorbitol accumulations in various tissues and oxidative stress, Eur. J. Med. Chem. 168 (2019) 154–175, https://doi.org/10.1016/j.ejmech.2019.02.036.

[40] M.G. Salem, Y.M.A. Aziz, M. Elewa, H.A. Elshihawy, M.M. Said, Synthesis and molecular modeling of novel non-sulfonylureas as hypoglycemic agents and selective ALR2 inhibitors, Bioorg. Med. Chem. 27 (2019) 3383–3389, https://doi.org/10.1016/j.bmc.2019.06.024.

[41] F. Da Settimo, G. Primofiore, C. La Motta, S. Salerno, E. Novellino, G. Greco, A. Lavecchia, S. Laneri, E. Boldrini, Spirohydantoin derivatives of thiopyrano[2,3-b]pyridin-4(4H)-one as potent in vitro and in vivo aldose reductase inhibitors, Bioorg. Med. Chem. 13 (2005) 491–499, https://doi.org/10.1016/j.bmc.2004.10.019.

[42] J. Inoue, Y.-S. Cui, L. Rodriguez, Z. Chen, P.F. Kador, Synthesis and aldose reductase inhibitory activities of novel dibenzocycloheptenone derivatives, Eur. J. Med. Chem. 34 (1999) 399–404, https://doi.org/10.1016/S0223-5234(99)80089-0.

[43] M. López-Lázaro, How many times should we screen a chemical library to discover an anticancer drug? Drug Discovery Today 2 (2015) 167–169, https://doi.org/10.1016/j.drudis.2014.12.006.

[44] O.A. Peña-Morán, M.L. Villarreal, L. Álvarez-Berber, A. Meneses-Acosta, V. Rodríguez-López, Cytotoxicity, post-treatment recovery, and selectivity analysis of naturally occurring podophyllotoxins from Bursera fagaroides var. fagaroides on breast cancer cell lines, Molecules 21 (2016) 1013, https://doi.org/10.3390/molecules21081013.

[45] C.A. Lipinski, F. Lombardo, B.W. Dominy, P.J. Feeney, Experimental and computational approaches to estimate solubility and permeability in drug discovery and development settings, Adv. Drug Deliv. Rev. 23 (1997) 3–25, https://doi.org/10.1016/S0169-409X(96)00423-1.

[46] E.M. Duffy, W.L. Jorgensen, Prediction of properties from simulations: free energies of solvation in hexadecane, octanol, and water, J. Am. Chem. Soc. 122 (2000) 2878–2888, https://doi.org/10.1021/ja993663t.

[47] A.K. Ghose, V.N. Viswanadhan, J.J. Wendoloski, A knowledge-based approach in designing combinatorial or medicinal chemistry libraries for drug discovery. 1. A qualitative and quantitative characterization of known drug databases, J. Comb. Chem. 1 (1999) 55–68, https://doi.org/10.1021/cc9800071.
[48] D.F. Veber, S.R. Johnson, H.-Y. Cheng, B.R. Smith, K.W. Ward, K.D. Kopple, Molecular properties that influence the oral bioavailability of drug candidates, J. Med. Chem. 45 (2002) 2615–2623, https://doi.org/10.1021/jm020017n.
[49] W.J. Egan, K.M. Merz, J.J. Baldwin, Prediction of drug absorption using multivariate statistics, J. Med. Chem. 43 (2000) 3867–3877, https://doi.org/10.1021/jm000292e.
[50] I. Muegge, S.L. Heald, D. Brittelli, Simple selection criteria for drug-like chemical matter, J. Med. Chem. 44 (2001) 1841–1846, https://doi.org/10.1021/jm015507e.
[51] Y.C. Martin, A bioavailability score, J. Med. Chem. 48 (2005) 3164–3170, https://doi.org/10.1021/jm0492002.
[52] J.B. Baell, G.A. Holloway, New substructure filters for removal of pan assay interference compounds (PAINS) from screening libraries and for their exclusion in bioassays, J. Med. Chem. 53 (2010) 2719–2740, https://doi.org/10.1021/jm901137j.
[53] A. Ece, F. Sevin, Exploring QSAR on 4-cyclohexylmethoxypyrimidines as antitumor agents for their inhibitory activity of cdk2, Letters in Drug Design & Discovery 7 (2010) 625–631, https://doi.org/10.2174/157018010792929612.
[54] T. Karakurt, A. Cukurovali, N.T. Subasi, A. Onaran, A. Ece, S. Eker, I. Kani, Experimental and theoretical studies on tautomeric structures of a newly synthesized 2,2′(hydrazine-1,2-diylidenebis(propan-1-yl-1-ylidene))diphenol, Chem. Phys. Lett. 693 (2018) 132–145, https://doi.org/10.1016/j.cplett.2018.01.016.
[55] K. Chan, N. Frankish, T. Zhang, A. Ece, A. Cannon, J. O'Sullivan, H. Sheridan, Bioactive indanes: insight into the bioactivity of indane dimers related to the lead anti-inflammatory molecule PH46A, J. Pharm. Pharmacol. 72 (2020) 927–937, https://doi.org/10.1111/jphp.13269.
[56] C. Yamali, H.I. Gul, M. Tugrak Sakarya, B. Nurpelin Saglik, A. Ece, G. Demirel, M. Nenni, S. Levent, A. Cihat Oner, Quinazolinone-based benzenesulfonamides with low toxicity and high affinity as monoamine oxidase-A inhibitors: Synthesis, biological evaluation and induced-fit docking studies, Bioorganic Chemistry 124 (2022) 105822, https://doi.org/10.1016/j.bioorg.2022.105822.
[57] A. Ece, Computer-aided drug design, BMC Chemistry 17 (2023) 26, https://doi.org/10.1186/s13065-023-00939-w.
[58] C. Türkeş, Carbonic anhydrase inhibition by antiviral drugs in vitro and in silico, Journal of Molecular Recognition 36 (2023) e3063.
[59] A. Atiya, A.B. Muhsinah, M. Alrouji, F.A. Alhumaydhi, W. Al Abdulmonem, M. A. Aljasir, S.E. Sharaf, M. Furkan, R.H. Khan, M. Shahwan, A. Shamsi, Unveiling promising inhibitors of superoxide dismutase 1 (SOD1) for therapeutic interventions, Int. J. Biol. Macromol. 253 (2023) 126684, https://doi.org/10.1016/j.ijbiomac.2023.126684.
[60] A. Shamsi, M. Furkan, R.H. Khan, M.S. Khan, M. Shahwan, D.K. Yadav, Comprehensive insight into the molecular interaction of rutin with human transferrin: Implication of natural compounds in neurodegenerative diseases, Int. J. Biol. Macromol. 253 (2023) 126643, https://doi.org/10.1016/j.ijbiomac.2023.126643.
[61] M.J. Cerelli, D.L. Curtis, J.P. Dunn, P.H. Nelson, T.M. Peak, L.D. Waterbury, Antiinflammatory and aldose reductase inhibitory activity of some tricyclic arylacetic acids, J. Med. Chem. 29 (1986) 2347–2351, https://doi.org/10.1021/jm00161a033.
[62] C. Türkeş, Y. Demir, Ş. Beydemir, Anti-diabetic properties of calcium channel blockers: inhibition effects on aldose reductase enzyme activity, Appl. Biochem. Biotechnol. 189 (2019) 318–329, https://doi.org/10.1007/s12010-019-03009-x.
[63] Y. Demir, H. Ceylan, C. Türkeş, Ş. Beydemir, Molecular docking and inhibition studies of vulpinic, carnosic and usnic acids on polyol pathway enzymes, J. Biomol. Struct. Dyn. 40 (2022) 12008–12021, https://doi.org/10.1080/07391102.2021.1967195.
[64] K.A. Johnson, R.S. Goody, The original Michaelis constant: translation of the michaelis-menten paper, Biochemistry 50 (2011) (1913) 8264–8269, https://doi.org/10.1021/bi201284u.
[65] C. Türkeş, Y. Demir, Ş. Beydemir, In vitro inhibitory activity and molecular docking study of selected natural phenolic compounds as AR and SDH inhibitors, ChemistrySelect 7 (2022) e202204050.
[66] M. Ishtikhar, E. Ahmad, Z. Siddiqui, S. Ahmad, M.V. Khan, M. Zaman, M.K. Siddiqi, S. Nusrat, T.I. Chandel, M.R. Ajmal, R.H. Khan, Biophysical insight into the interaction mechanism of plant derived polyphenolic compound tannic acid with homologous mammalian serum albumins, Int. J. Biol. Macromol. 107 (2018) 2450–2464, https://doi.org/10.1016/j.ijbiomac.2017.10.136.
[67] C. Türkeş, Y. Demir, A. Biçer, G.T. Cin, M.S. Gültekin, Ş. Beydemir, Exploration of some bis-sulfide and bis-sulfone derivatives as non-classical aldose reductase inhibitors, ChemistrySelect 8 (2023) e202204350, https://doi.org/10.1002/slct.202204350.
[68] T. Mosmann, Rapid colorimetric assay for cellular growth and survival: Application to proliferation and cytotoxicity assays, J. Immunol. Methods 65 (1983) 55–63, https://doi.org/10.1016/0022-1759(83)90303-4.
[69] S.M. Ali, F. Nabi, M. Furkan, M. Hisamuddin, S. Malik, S.M. Zakariya, I. Rizvi, V. N. Uversky, R.H. Khan, Tuning the aggregation behavior of human insulin in the presence of luteolin: An in vitro and in silico approach, Int. J. Biol. Macromol. 237 (2023) 124219, https://doi.org/10.1016/j.ijbiomac.2023.124219.
[70] A. Buza, C. Türkeş, M. Arslan, Y. Demir, B. Dincer, A.R. Nixha, Ş. Beydemir, Discovery of novel benzenesulfonamides incorporating 1,2,3-triazole scaffold as carbonic anhydrase I, II, IX, and XII inhibitors, Int. J. Biol. Macromol. 239 (2023) 124232, https://doi.org/10.1016/j.ijbiomac.2023.124232.
[71] Ö. Güleç, C. Türkeş, M. Arslan, Y. Demir, B. Dincer, A. Ece, Ş. Beydemir, Novel beta-lactam substituted benzenesulfonamides: in vitro enzyme inhibition, cytotoxic activity and in silico interactions, J. Biomol. Struct. Dyn. (2023) 1–19, https://doi.org/10.1080/07391102.2023.2240889.
[72] C. Kakakhan, C. Türkeş, Ö. Güleç, Y. Demir, M. Arslan, G. Özkemahlı, Ş. Beydemir, Exploration of 1,2,3-triazole linked benzenesulfonamide derivatives as isoform selective inhibitors of human carbonic anhydrase, Bioorg. Med. Chem. 77 (2023) 117111, https://doi.org/10.1016/j.bmc.2022.117111.
[73] Schrödinger Release 2023-3: QikProp, Schrödinger, LLC, New York, NY, 2023.
[74] S.U. Kumar, C.G. Priya Doss, Computational investigation to identify potent inhibitors of the GTPase-Kirsten RAt sarcoma virus (K-Ras) mutants G12C and G12D, Comput. Biol. Med., 139 (2021) 104946, https://doi.org/10.1016/j.compbiomed.2021.104946.
[75] A. Daina, O. Michielin, V. Zoete, SwissADME: a free web tool to evaluate pharmacokinetics, drug-likeness and medicinal chemistry friendliness of small molecules, Scientific Rep., 7 (2017) 42717, https://doi.org/10.1038/srep42717.
[76] M. Shahwan, N. Hassan, A. Ashames, M. Alrouji, F. Alhumaydhi, W. Al Abdulmonem, A.B. Muhsinah, M. Furkan, R.H. Khan, A. Shamsi, A. Atiya, PF543-like compound, a promising sphingosine kinase 1 inhibitor: Structure-based virtual screening and molecular dynamic simulation approaches, Int. J. Biol. Macromol., 245 (2023) 125466, https://doi.org/10.1016/j.ijbiomac.2023.125466.
[77] J. Natesh, P. Mondal, D. Penta, A.A. Abdul Salam, S.M. Meeran, Culinary spice bioactives as potential therapeutics against SARS-CoV-2: Computational investigation, Comput. Biol. Med., 128 (2021) 104102, https://doi.org/10.1016/j.compbiomed.2020.104102.
[78] T.I. Chandel, M. Zaman, M.V. Khan, M. Ali, G. Rabbani, M. Ishtikhar, R.H. Khan, A mechanistic insight into protein-ligand interaction, folding, misfolding, aggregation and inhibition of protein aggregates: An overview, Int. J. Biol. Macromol. 106 (2018) 1115–1129, https://doi.org/10.1016/j.ijbiomac.2017.07.185.
[79] L. Zhang, H. Zhang, Y. Zhao, Z. Li, S. Chen, J. Zhai, Y. Chen, W. Xie, Z. Wang, Q. Li, X. Zheng, X. Hu, Inhibitor selectivity between aldo–keto reductase superfamily members AKR1B10 and AKR1B1: Role of Trp112 (Trp111), FEBS Lett. 587 (2013) 3681–3686, https://doi.org/10.1016/j.febslet.2013.09.031.
[80] Schrödinger Release 2023-3: Small-Molecule Drug Discovery Suite, Schrödinger, LLC, New York, NY, 2023.
[81] Schrödinger Release 2023-3: Protein Preparation Wizard, Schrödinger, LLC, New York, NY, 2023.
[82] C. Türkeş, M. Arslan, Y. Demir, L. Çoçaj, A.R. Nixha, Ş. Beydemir, N-substituted phthalazine sulfonamide derivatives as non-classical aldose reductase inhibitors, J. Mol. Recognit. 35 (2022) e2991.
[83] C. Lu, C. Wu, D. Ghoreishi, W. Chen, L. Wang, W. Damm, G.A. Ross, M.K. Dahlgren, E. Russell, C.D. Von Bargen, R. Abel, R.A. Friesner, E.D. Harder, OPLS4: Improving Force Field Accuracy on Challenging Regimes of Chemical Space, Journal of Chemical Theory and Computation 17 (2021) 4291–4300, https://doi.org/10.1021/acs.jctc.1c00302.
[84] Schrödinger Release 2023-3: LigPrep, Schrödinger, LLC, New York, NY, 2023.
[85] Schrödinger Release 2023-3: Glide, Schrödinger, LLC, New York, NY, 2023.
[86] R.A. Friesner, J.L. Banks, R.B. Murphy, T.A. Halgren, J.J. Klicic, D.T. Mainz, M. P. Repasky, E.H. Knoll, M. Shelley, J.K. Perry, D.E. Shaw, P. Francis, P.S. Shenkin, Glide: A new approach for rapid, accurate docking and scoring. 1. Method and assessment of docking accuracy, J. Med. Chem. 47 (2004) 1739–1749, https://doi.org/10.1021/jm0306430.
[87] Schrödinger Release 2023-3: Desmond Molecular Dynamics System, DE Shaw Research, Schrödinger, LLC, New York, NY, 2023.
[88] A. Imran, M. Tariq Shehzad, T. al Adhami, K. Miraz Rahman, D. Hussain, R.D. Alharthy, Z. Shafiq, J. Iqbal, Development of coumarin-thiosemicarbazone hybrids as aldose reductase inhibitors: Biological assays, molecular docking, simulation studies and ADME evaluation, Bioorg. Chem., 115 (2021) 105164, https://doi.org/10.1016/j.bioorg.2021.105164.